THE REPUBLIC OF UZBEKISTAN HIGH AND SECONDARY

SPECIAL EDUCATION DEPARTMENT

TASHKENT STATE PEDAGOFICAL UNIVERSITY NAMED AFTER NIZAMI

PHYSICS AND MATHEMATICS FACULTY

"Allowed to assertion"

The dean of faculty doctor of

science _____ D.I.Yunusova

"____ " _____ 2013 year

5140200-"Physics and astronomy" study field

The fourth year student

TUKHTAEV Boburbek Jamoliddin ugli

Theme: THE MECHANISM OF FLARING CORONAL BRIGHT POINTS

FINAL QUALIFYING WORK OF BACHELOR

Graduate: _____ Tukhtaev B.

Instructor: Proffessor_____ Sattorov I.

Reviewer: Ph.D. _____ Sattarova B.

Reviewer: S.S.R. _____ Sherdanov Ch.

"____ " _____ 2013 year

Tashkent – 2013

Content

INTRODUCTION

Nowadays scientific research are being huge attention coincide with developing educational system by every government. They have gained several achievement through these researches and methods. Some of them were awarded by country with variety of presents.

With astronomical data arriving at essentially every wavelength of the electromagnetic spectrum, this is a fascinating time for astronomy and astrophysics worldwide. Johns Hopkins astrophysicists lead research across the entire range of the discipline, from cosmology to galactic structure to planets, using observational, numerical and theoretical methods. JHU astronomers along with members of the Space Telescope Science Institute just across the street from our building jointly form one of the largest astrophysics communities in the country. The past two years have brought many exciting developments for the astrophysics researchers in our department. Professor Adam Riess received the 2011 Nobel Prize in physics for the discovery of the accelerated expansion of the Universe. The department continued its commitment to leadership in large-scale astronomical surveys and joined the Prime Focus Spectrograph project. Several new astrophysics faculty joined our department: professor Marc Kamionkowski, assistant professors Tobias Marriage, Nadia Zakamska and Brice Menard, and Homewood Professor Joseph Silk in a shared appointment.

Our young should be educated well in order to work this kind of researches. Astrophysics is being taught in universities and colleges in current days. Because it is impossible to perform research without theoretical knowledge and it looks like that blind person is walking on the street alone.

Moreover, in modern society not only researches are being developed on educational system, but also space researches are being held by government. For example recent investigations have shown that there are three habitual planets in space. The same time with these research scientists are learning solar system. In my diploma work some parts of solar system have been learnt. Several results were analyzed and learned.

All in all the theme of diploma work is prominent and it is dedicated to learn the mechanism of coronal bright points.

Object of the final qualifying work

Object of the study is – evolution of solar corona's fine structure, which is proposed as source coronal heating.

Subject of the final qualifying work

Subject of the study is evolution of coronal bright points in differ parts of solar corona (quiet, active coronal parts and coronal holes).

Purpose of the final qualifying work

The present work applies MCC to the case of a magnetic bipole. This leads to predictions for the interaction distance and heating power for magnetic bipoles in every possible configuration. The predicted size and power compare favorably with the values inferred from observations of XBPs. The exact scaling can be tested against existing or future XBP data. Furthermore, the model leads to several other predictions, such as an angular discrepancy between the axis of the bipole and the XBP, which can be tested.

The mession of final qualifying work:

1**.** To choose and collect literature which is belong to theme

2. To search and gather information, which is belong to theme, from internet

3. To learn suitable information about theme

4. Planning the scheme of final qualifying work

5. To equip final qualifying work according to scheme

6. Preparing the final qualifying work to assert

ABSTRACT

X-ray bright points are believed to result from the interaction of two small magnetic features of opposite polarity. As these features move apart, flux interconnecting them can become disconnected and joined to the overlying magnetic field. For features moving toward one another this process will occur in reverse. In either case this magnetic reconnection occurs at the separator field line. Assuming that reconnection can occur only after it is "triggered," the process will heat the plasma nearby the separator, thereby giving rise to the X-ray brightening. This can be quantified using a recent model of current sheet formation and reconnection along separators. Application of this model predicts the heating from reconnection based on the observable magnetic quantities of flux, field strength, and polar separation. In addition, the model predicts morphological aspects of the bright points such as the apparent angle between the axes of the X-ray loop and the magnetic bipole.

CHAPTER 1. SOLAR CORONA AND CORONAL BRIGHT POINTS

1.1. Structure of coronal bright points

Studying the Corona

The corona is that region of the solar atmosphere lying above the chromosphere. As seen in photographs taken during a total eclipse, it is the large halo of white, glowing gas extending out a few solar radii (millions of kilometers) beyond the dark limb of the Moon. At times when an eclipse is not in progress, specially designed refracting telescopes, called coronagraphs, that block out light from the photosphere are used to observe the corona.

Compared with the many hours of almost continuous surveillance accumulated in satellite studies over the last 20 years, eclipse studies have yielded not more than a few hours of observations (an eclipse seldom lasts longer than a few minutes). Even coronagraphic studies, which have greatly increased observing time, cannot match the time coverage and resolution of satellite observations from above the atmosphere. In February of 1980, the launching of the Solar Maximum Mission spacecraft, one of the most sophisticated and complex satellites ever built, provided the opportunity to keep watch on the Sun during its period of maximum surface activity. However, in November of that year, Solar Max lost its attitude-control system, so that the craft could no longer point its eight instruments at interesting portions of the solar surface. Then in April of 1984, the crew of the Space Shuttle Challenger were able to wrestle Solar Max into the cargo bay of Challenger for repair (chapter opening). This first successful repair of a satellite in orbit opens a new era for space observatories, in that in the future they will be repaired or serviced in orbit or even returned to the ground for modification. Properly attended, Solar Max may well last into the 1990s or almost a complete solar cycle of 11 years.

The Coronal Spectrum. Approximately 30 emission lines have been identified in the visible part of the coronal spectrum, and many hundreds of emission lines are known in the ultraviolet and X-ray spectrum. They originate

in highly excited ions of familiar elements, such as iron, from which several to as many as 15 electrons have been stripped in the corona's extremely hot, tenuous gases. (It takes temperatures from many hundreds of thousands up to several million degrees to sustain such a degree of ionization.)

From millimeter to meter wavelengths there is a wide spectral window in the Earth's atmosphere that lets in radio radiation. The Sun, when quiet and undisturbed, normally emits thermal (blackbody) radiation, which is characteristic of a million-degree corona. When the Sun is disturbed, as when solar flares are occurring, nonthermal radio emission is added to the thermal component, and it can be quite intense.

Coronal Structure. There are several lines of evidence, besides the coronal spectrum, that confirms a rise in temperature through the chromosphere into the corona. Since heat flows from high to low temperature regions, then clearly energy must be pumped by some mechanism from the low-temperature photosphere to the high-temperature corona. For a number of years astronomers thought that the corona's high temperature resulted from energy carried into the corona by mechanical waves starting in the turbulent hydrogen convection zone below the photosphere.

As evidence grew that the magnetic fields of the photosphere and chromosphere were highly localized and very intense, it seemed hard to ignore the possibility that these magnetic fields extending up into the corona were part of the coronal heating process. When X-ray pictures showed that the corona was divided into active regions and hole regions primarily because of the structures of their magnetic fields, it became readily apparent that most, if not all, of the heating involves magnetic fields. The heating is produced by the direct dissipation of the energy stored in magnetic fields into thermal energy in the coronal gas. The lower parts of the chromosphere, however, are still thought to be heated by mechanical waves.

Eclipse pictures of the corona provide evidence for the importance of magnetic fields in structuring the corona. In white-light photographs one can see

that the corona is irregular and structured. Beautiful, long streamers extend outward in the Sun's equatorial regions. Near sunspot maximum the corona is nearly circular, with streamers radiating out in all directions. Near sunspot minimum, the corona extends farther out in the equatorial region and terminates rather abruptly, with short, thin plumes curving out of polar areas.

Because coronal gases are almost transparent, we often are looking through several structures at once in eclipse pictures, which blurs the details. This is why direct photographs in X-ray and extreme ultraviolet wavelengths, where we look down on top of coronal structures, are so valuable to the study of the corona. To photograph the corona directly, we must observe in the 10 to 900 A (X-ray to extreme ultraviolet) wavelength region, where radiation from the much hotter corona overwhelms the short-wavelength radiation of the photosphere. But X-ray or ultraviolet pictures must be taken from space because the Earth's atmosphere absorbs these short wavelengths. In X-ray and ultraviolet pictures the corona appears highly inhomogeneous and generally asymmetrical, and it varies over time on both short and long time scales.

There are three different types of structural regions that collectively characterize the entire solar corona: Coronal holes and coronal active regions are two of them, and they are reasonably well defined in terms of observational characteristics; the third is the coronal quiet regions, which are not well defined. Coronal holes are regions of slightly lower temperatures and significantly lower densities, with magnetic fields of about 10 gauss whose lines open out into interplanetary space. Rays and polar plumes extend out of them away from the Sun. Coronal holes are also thought to be the source of most of the subatomic particles in the solar wind. Coronal active regions, however, are extremely different from coronal holes. They consist of loop structures, they are somewhat hotter and much denser regions of the corona, and their magnetic fields of about 100 gauss having field lines that loop back into the Sun instead of extending outward as in the case of coronal holes. Between these two extremes are the ill-

defined coronal quiet regions, which appear to be something in between. There are also many small, bright points visible in X-ray pictures.

1.2. Magnetic field in solar corona

The magnetic reconnection theory relies on the solar magnetic field to induce electric currents in the solar corona. The currents then collapse suddenly, releasing energy as heat and wave energy in the corona. This process is called "reconnection" because of the peculiar way that magnetic fields behave in a plasma (or any electrically conductive fluid such as mercury or seawater). In a plasma, magnetic field lines are normally tied to individual pieces of matter, so that the topology of the magnetic field remains the same: if a particular north and south magnetic pole are connected by a single field line, then even if the plasma is stirred or if the magnets are moved around, that field line will continue to connect those particular poles. The connection is maintained by electric currents that are induced in the plasma. Under certain conditions, the electric currents can collapse, allowing the magnetic field to "reconnect" to other magnetic poles and release heat and wave energy in the process.

Magnetic reconnection is hypothesized to be the mechanism behind solar flares, the largest explosions in our solar system. Furthermore, the surface of the Sun is covered with millions of small magnetized regions 50–1,000 km across. These small magnetic poles are buffeted and churned by the constant granulation. The magnetic field in the solar corona must undergo nearly constant reconnection to match the motion of this "magnetic carpet", so the energy released by the reconnection is a natural candidate for the coronal heat, perhaps as a series of "microflares" that individually provide very little energy but together account for the required energy.

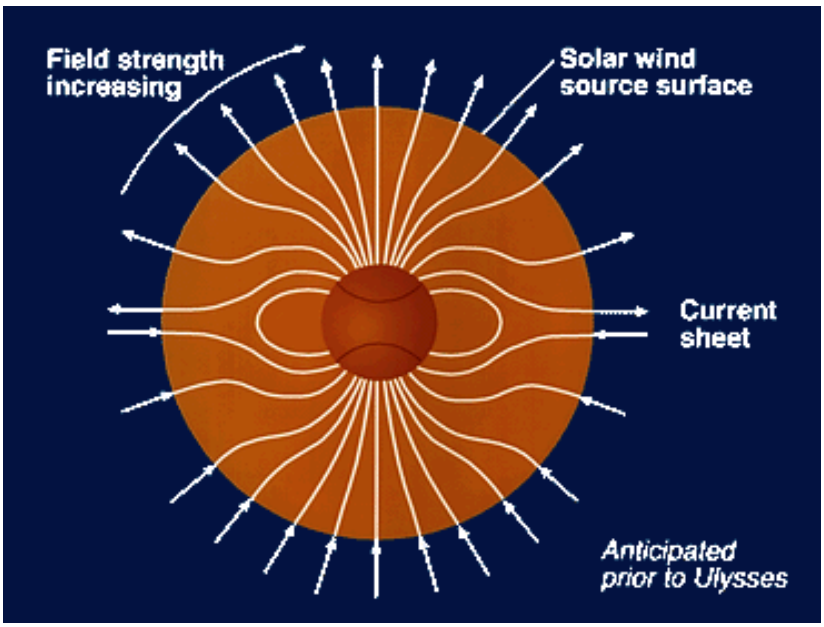

Figure 1.1.
In that picture the direction of magnetic field and its distribution are described on solar disc. I addition their motion are illustrated.

The idea that nanoflares might heat the corona was put forward by Eugene Parker in the 1980s but is still controversial. In particular, ultraviolet telescopes such as TRACE and SOHO/EIT can observe individual micro-flares as small brightenings in extreme ultraviolet light, but there seem to be too few of these small events to account for the energy released into the corona. The additional energy not accounted for could be made up by wave energy, or by gradual magnetic reconnection that releases energy more smoothly than micro-flares and therefore doesn't appear well in the TRACE data. Variations on the micro-flare hypothesis use other mechanisms to stress the magnetic field or to release the energy, and are a subject of active research in 2005.(wekipedia)

Wilcox Solar Observatory (WSO)	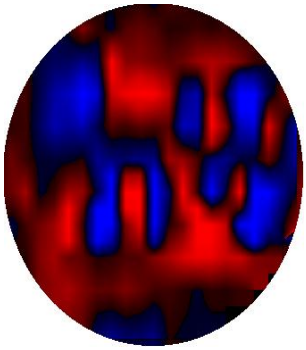
National Solar Observatory SOLIS (NSO)	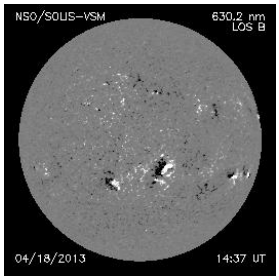
Mt. Wilson Observatory (MWO)	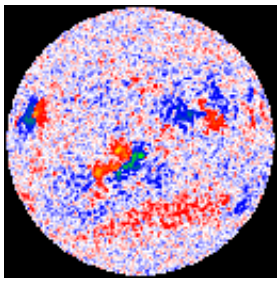
Realtime GONG magnetogram page at SSL, UCB.	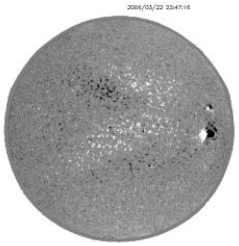

Figure 1.2 shows Sources of Magnetograms and the latest images : On the left side Sources of Magnetograms are written, on the right side their latest picture are shown correspondingly with their sources.

Definitive Measurement of the Coronal Magnetic Field. The magnetic field in the solar corona is generally believed to be responsible for a wide range of phenomena from being the carrier of MHD waves to heat the corona, to producing the gyro-synchrotron radiation in the radio wavelength range. Yet, there are scarcely any direct measurements of the coronal magnetic field to date. Early magnetograph observations in the "green" Fe XIIII 5303 coronal emission line (Harvey 1969) gave us a pretty good idea of just how difficult these measurements could be. The strongest flux he detected in the rising phase of a solar cycle (1967, 1968) was only 13 20 G. More recent spectro-polarimetric measurements (Kuhn 1995) placed an upper limit of 50 G, using the near-infrared Fe XIII 10797 line. Linear polarization observations in the 1980's (Querfeld and Smartt 1984, Arnaud and Newkirk 1987) were more successful in mapping the direction of the coronal magnetic fields. However, because the linear polarization of coronal emission lines (CEL) is not sensitive to the strength of the magnetic field, no quantitative information of the magnetic flux can be derived from these linear polarization experiments. We are faced with the dilemma of believing that magnetic fields exist in the solar corona and play a crucial rule in almost all coronal activities; numerous new theoretical investigations and results from current space-borne experiments (SoHO, TRACE) only reinforce this conviction, while definitive quantitative measurement of the magnetic field is conspicuously missing. In order to further advance our knowledge of the solar corona, direct measurement of the coronal magnetic field strength and configuration is indispensable.

To first order approximation, the CEL linear polarization measurement only provides information on the orientation of the magnetic field vector. Information about the magnetic field strength (flux) is contained only in the circular polarization of the CELs (Cassini and Judge 1999, Lin and Cassini 1999). Measurement of the Stokes V signal due to the coronal magnetic field is one of the most difficult experiments in the field of observational solar astronomy. The magnetic field strength is expected to be very small, around

10 G; therefore, the degree of circular polarization is expected to be minute. The high coronal temperature broadens the spectral lines, further reducing the Stokes V signal. Under coronal conditions, the expected Stokes V amplitude is only 10-3 Iline or smaller. Also, the linear polarization of the CELs is typically two orders of magnitude higher than the circular polarization. Therefore, measurement of the coronal Stokes V signal is only feasible with a very sensitive polarimeter with extremely small instrumental (telescope and polarimeter) polarization cross talk. The low photon flux of the emission line solar corona (~~10-5 disk intensity) also aggravates the situation. Nevertheless, encouraged by recent successes of high-precision spectro-polarimetric observations of weak photospheric magnetic fields, Haosheng Lin (NSO), Steve Tomczyk (HAO), and Matt Penn (Cal State, Northridge) attempted to obtain a quantitative measurement of the coronal magnetic field.

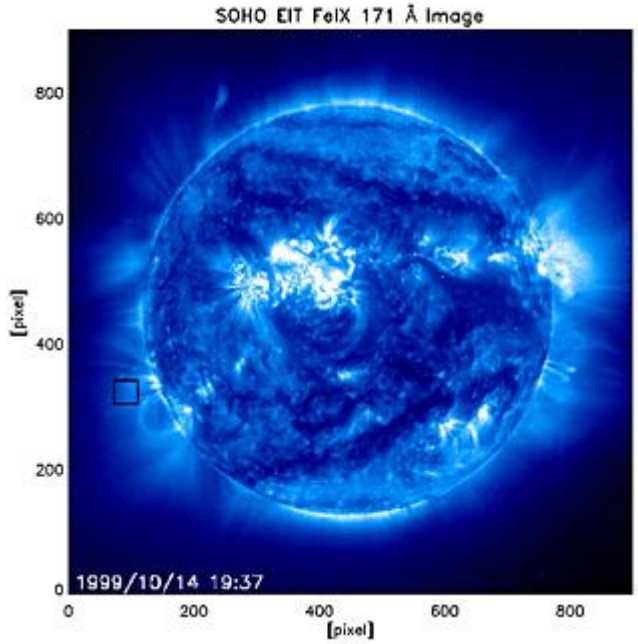

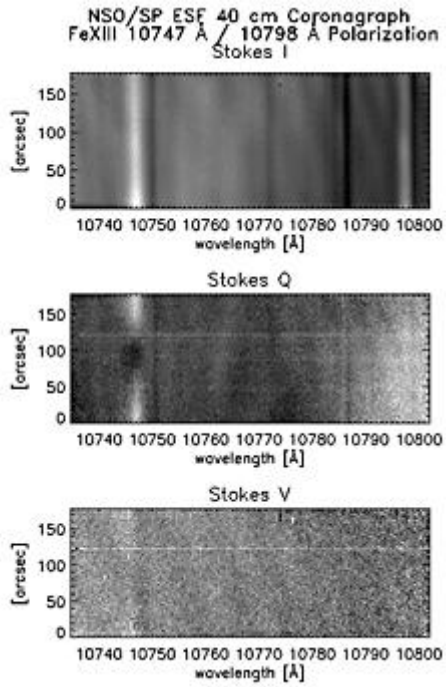

Figure 1.3 Figure 1.4

Figure 1.3. The SoHO EIT Fe IX 171 Å image shows the structure of the solar corona near the time of the IR observation. The region marked by the square box is the target area observed by the IR polarimeter. The Stokes Q spectra show variation across the field of view, indicating magnetic field

variation across the FOV. The Stokes V spectra show a faint anti-symmetric structure across the FOV at the location of the Fe XIII 10747 Å line. The averaged Stokes V spectrum is shown in Figure 1.4. (SoHO/EIT image courtesy of SoHO/EIT consortium. SoHO is a project of international cooperation between ESA and NASA.)

The NSO/Sac Peak Evans Solar Facility's (ESF) 40-cm coronagraph was used for the experiment. Lin and colleagues designed and built a new Echelle spectrograph optimized for the Fe XIII 10747 and 10798 line pair. A liquid crystal variable retarder polarimeter and the Michigan State University NICMOS 3 IR camera were used to analyze and record the Stokes spectra. To eliminate telescope polarization cross talk, the polarimeter was mounted directly behind the O1 focus of the coronagraph before any of the polarization cross talk generating reflecting optics. An iterative retardation tuning algorithm was developed to minimize the linear to circular polarization cross talk within the polarimeter itself. With these special considerations in minimizing the instrumental cross talk, the linear to circular cross talk is typically at the low 10-3 level.

The first positive detection of a coronal Stokes V signal was achieved on 14 October 1999, observing in a region of the solar corona with strong (83 millionth of disk-center intensity) Fe XIIII 5303 green-line emission. Several attempts during subsequent days in weaker green-line regions yielded weak Stokes V signals that were barely above the noise level. Figure 1.3 shows the IR Fe XIII 10747 and 10798 emission line I, Q, and V polarization spectra of the October 14 observation, and the SoHO EIT Fe IX 171 image to indicate the IR target region (the square box in the EIT image). The integration times for the Stokes Q and V frames are both 20 minutes, while the total observing time was 70 minutes. A total of 2,048 exposures were taken for this observation. The Stokes Q spectrum image clearly shows the linear polarization of both the Fe XIII 10747 and 10798 lines. The anti-symmetric Stokes V signal is only barely discernible in the circular polarization spectrum image. To improve the signal-

to-noise ratio of the Stokes V signal, we averaged over the full frame to generate an averaged Stokes V profile, shown with the averaged Stokes Q profile in Figure 1.3. Here, the anti-symmetric signature of the Stokes V profile is unmistakable. There was no evidence of Stokes Q to V cross talk in the image. A magnetic flux of 33 0.7 (3) G was derived from this Stokes V spectrum using the standard magnetograph formula. The alignment effect correction to the Stokes V profile (Cassini and Judge 1999, Lin and Cassini 1999) was not applied since we did not measure the full Stokes vector. A second detection was obtained on 23 October 1999, when a large active region just rotated behind the west limb of the Sun, which also yielded strong (79 millionths) green line intensity. The amplitude of the Stokes V signal of the October 23 observation was smaller compared to the October 23 measurement in line intensity units, but due to better sky conditions (13 millionths) and longer integration time (34 minutes for each Stokes state, 150 minutes total observing time), it was possible to detect a weak Stokes V signal. A magnetic flux of 10 0.5 (3) G was derived from this region.

These preliminary results provide the first definitive quantitative measurements of the coronal magnetic field, which will be an important input to all the theoretical modeling of the solar corona. Future measurements with improved signal-to-noise ratio, spatial coverage, and temporal resolution will make major contributions to the advancement of the physics of the solar and stellar coronae.

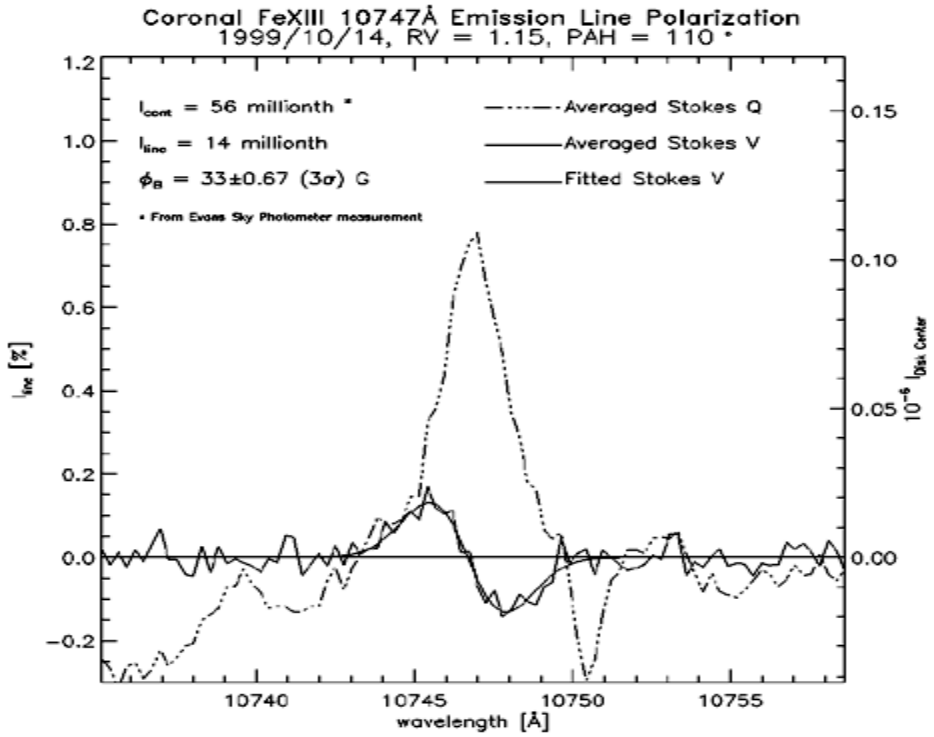

Figure 1.5. The Stokes Q and V profiles averaged over the entire field of view in Figure 1.3. The magnetic anti-symmetric profile of the Stokes V spectrum is clearly shown. The thin solid line is the fitted Stokes V profile. The observers did not have disk-center intensity calibration data for this observation, and the calibration to disk-center intensity was obtained from sky brightness measurement using the Evans' sky photometer.

1.3. Coronal bright points

One of the three key features of the Sun when seen in X-rays, the others being active regions and coronal holes. Unlike active regions, coronal bright points are distributed at all latitudes on the solar disk. Bright points have a central core around 10 000 km wide and mostly occur above areas of opposite magnetic polarity on the photosphere; when the regions of opposite polarity encounter each other and cancel out, energy is released that heats the gas above the photosphere to 1–2 million K. Bright points also occur when newly emerged magnetic field reacts with the pre-existing magnetic field in the corona, again with the release of magnetic energy to heat the gas. Coronal bright points have

typical lifetimes of a day. They are often referred to as X-ray bright points or EUV bright points, according to the wavelength at which they are observed.

Bright points are small active regions spread over the whole solar disk. X-ray bright points were first detected in April 8, 1969 during a rocket flight.

The fraction of the solar surface covered by bright points varies with the solar cycle. They are associated with small bipolar regions of the magnetic field. Their average temperature ranges from 1.1 MK to 3.4 MK. The variations in temperature are often correlated with changes in the X-ray emission.

X-ray bright points. X-ray bright points are believed to result from the interaction of two small magnetic features of opposite polarity. As these features move apart, flux interconnecting them can become disconnected and joined to the overlying magnetic field. For features moving toward one another this process will occur in reverse. In either case this magnetic reconnection occurs at the separator field line. Assuming that reconnection can occur only after it is "triggered," the process will heat the plasma nearby the separator, thereby giving rise to the X-ray brightening. This can be quantified using a recent model of current sheet formation and reconnection along separators. Application of this model predicts the heating from reconnection based on the observable magnetic quantities of flux, field strength, and polar separation. In addition, the model predicts morphological aspects of the bright points such as the apparent angle between the axes of the X-ray loop and the magnetic bipole.

Soft X-ray filtergrams show the presence on the Sun of large numbers of small, closed regions of coronal emission. These features, called 'X-ray bright points' correspond to small, short-lived regions of emerging magnetic flux. As a function of size or lifetime they form a broad spectrum of activity which is continuous with the active regions. The shape of the Sun's activity spectrum is such that most of all magnetic flux emerging at the surface comes in the form of bright points. From this viewpoint, active regions may be viewed as the long lifetime tail end of the bright point spectrum. Examination of soft X-ray data obtained from 1970 to 1978 shows that the number of bright points appears to be

anticorrelated with traditional activity indices such as sunspot number; the anticorrelation persists after corrections are made for obscuration by active regions. Comparison of X-ray data with KPNO magnetograms shows that to within a factor of 2, the average total amount of magnetic flux emerging over the full Sun is constant through the entire period of observation. The solar cycle therefore appears to be more an oscillation in the wavenumber distribution of emerging flux than of the total quantity of magnetic flux produced.

X-ray bright points (XBPs) are small (60'') isolated pointlike or looplike features found most often in coronal holes and quiet-Sun regions. Originally observed in soft X-ray images, they are also observed in radio and EUV line emission It has been shown that the locations of XBPs correlate strongly with the locations of pairs of opposing magnetic elements, called bipoles, found in magnetograms Kankelborg This has led to the hypothesis that XBPs result from some form of interaction between opposing magnetic poles.

Typical XBPs are loops 20 Mm (30'') long that last for lifetimes ranging from 2 to 48 hours. In a survey of Skylab S-054 data the average lifetime was determined to be 8 hours. The X-ray luminosity can fluctuate over timescales as short as 10 minutes. In addition to the power radiated in X-rays and the EUV, models suggest that the coronal plasma also loses power by thermal conduction into the relatively cooler. These observed and inferred losses must be balanced by a source of energy (heating) to keep the XBP bright over its lifetime. Observed variability indicates that this heating source is at least partly impulsive. Kankelborg et al. (1997) applied a steady state energy balance model to 23 XBPs observed with a rocket-borne FUV instrument on 1991 May 13. The model can be used to infer the total heating power required by each XBP. Computed power requirements range from 4×1022 to 4×1024 ergs s^{-1} in the sample of 23 XBPs; the median value is 1024 ergs s^{-1}.

The present work applies MCC to the case of a magnetic bipole. This leads to predictions for the interaction distance and heating power for magnetic bipoles in every possible configuration. The predicted size and power compare

favorably with the values inferred from observations of XBPs. The exact scaling can be tested against existing or future XBP data. Furthermore, the model leads to several other predictions, such as an angular discrepancy between the axis of the bipole and the XBP, which can be tested.

Morphology of X-Ray bright points. The model above attributes XBPs to reconnection in a magnetic bipole. We have shown that reconnection would naturally liberate magnetic energy, which would, in turn, lead to X-ray brightening along affected magnetic field lines σ. The magnetic field lines most affected will be those closest to the reconnection site: the separator field line. Thus, we expect the morphology of an XBP to reflect the morphology of the separator.

Viewed from above (see Fig. 1.6) the separator makes a lazy "S" shape connecting the two null points (Fig. 1.6). It is worth recalling that a potential magnetic field is being used so the curvature cannot be the result of current (Priest & Milne 1980). The magnetic field is sheared, even in this potential field. At low altitudes the magnetic field is directed along the bipole axis, while higher up the background field dominates. The separator σ follows each of these directions over its length, leading to its S shape. The axis of the separator is intermediate between the bipole and the background.

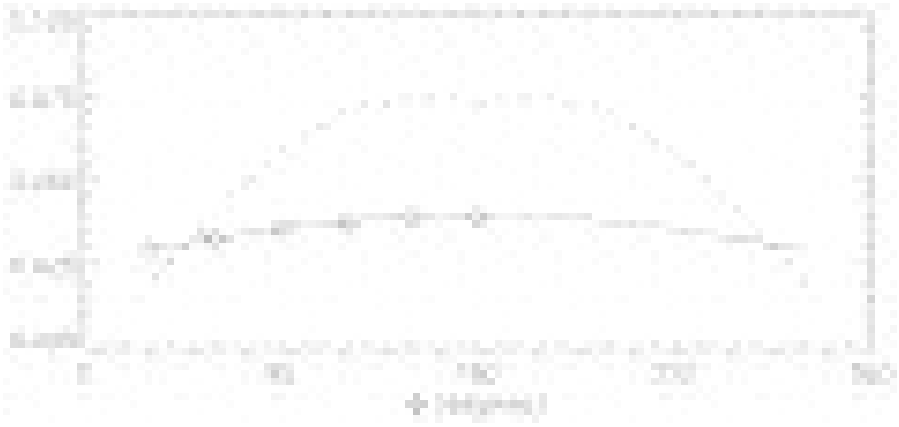

Figure 1.6

This S-shaped separator makes an angle Δφ with respect to the axis of the bipole itself (i.e., P and N) since its ends, the null points, are necessarily offset from the poles. This offset angle is an important prediction of the

separator model; simpler models do not often distinguish between the bipole and the X-ray loop. Significantly such an offset has been noted in observations of X-ray bright points. Important constraints may be placed on the separator model by measurements of these offset angles.

The value of the theoretical offset angle depends on the definition of the separator axis. Defining a separator axis connecting the null points leads to an offset $\Delta\varphi$. Choosing the apex of the separator leads to a different angle $\Delta\varphi'$ (see Fig. 1.6). In practice these two offsets are not very different. Figure 1.7 shows the direction of each axis at different points in parameter space. The offset $\Delta\varphi$ corresponds to the angle between this axis and the radial. For angles $|\varphi| > 90°$ these offsets can be significant, becoming $|\Delta\varphi|=|\Delta\varphi'|= 90°$ at the $\varphi= 180°$ line. Conversely, when the bipole and the background are nearly aligned, $|\varphi| < 90°$, the offset angle is not great.

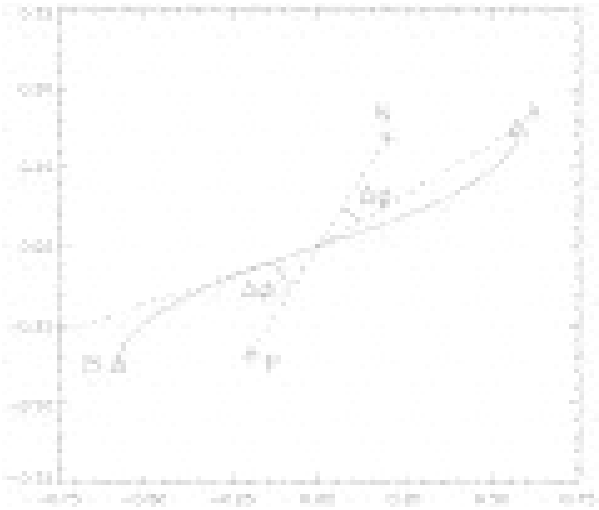

Figure 1.7

Dynamics of Coronal Bright Points as seen by Sun Watcher.

At that work Sun Watcher are used using Active Pixel System detector and Image Processing (SWAP), Atmospheric Imaging Assembly AIA), and Helioseismic and Magnetic Imager (HMI)

The \textit{Sun Watcher using Active Pixel system detector and Image Processing}(SWAP) on board the \textit{PRoject for OnBoard Autonomy\todash 2} (PROBA\todash 2) spacecraft provides images of the solar corona in EUV channel centered at 174 \AA. These data, together with

\textit{Atmospheric Imaging Assembly} (AIA) and the \textit{Helioseismic and Magnetic Imager} (HMI) on board \textit{Solar Dynamics Observatory} (SDO), are used to study the dynamics of coronal bright points. The evolution of the magnetic polarities and associated changes in morphology are studied using magnetograms and multi-wavelength imaging. The morphology of the bright points seen in low-resolution SWAP images and high-resolution AIA images show different structures, whereas the intensity variations with time show similar trends in both SWAP 174 and AIA 171 channels. We observe that bright points are seen in EUV channels corresponding to a magnetic-flux of the order of 10^{18} Mx. We find that there exists a good correlation between total emission from the bright point in several UV\todash EUV channels and total unsigned photospheric magnetic flux above certain thresholds. The bright points also show periodic brightenings and we have attempted to find the oscillation periods in bright points and their connection to magnetic flux changes. The observed periods are generally long (10\todash 25 minutes) and there is an indication that the intensity oscillations may be generated by repeated magnetic reconnection.

Coronal holes are the polar regions which look dark in the X-rays since they do not emit much radiation. These are wide zones of the Sun where the magnetic field is unipolar and opens towards the interplanetary space. The high speed solar wind arises mainly from these regions.

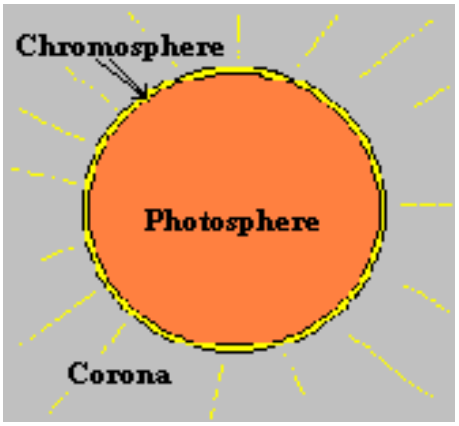

Figure 1.8

That figure gives information about the structure on solar. In the first layer if Chromosphere and it can aproximately reveal the Solar corona. The next layer which is inside of sun is photosphere and it is consists main part of the sun.

In the UV images of the coronal holes, some small structures, similar to elongated bubbles, are often seen as they were suspended in the solar wind. These are the coronal plumes. More exactly, they are long thin streamers that project outward from the Sun's north and south poles.

Coronal event	**Typical time-scale**	**Typicallength-scale (Mm)**
Active region flare	10 to 10,000 seconds	10–100
X-ray bright point	Minutes	1–10
Transient in large-scale structures	from minutes to hours	~100
Transient in interconnecting arcs	from minutes to hours	~100
Quiet Sun	from hours to months	100–1,000
Coronal hole	several rotations	100–1,000

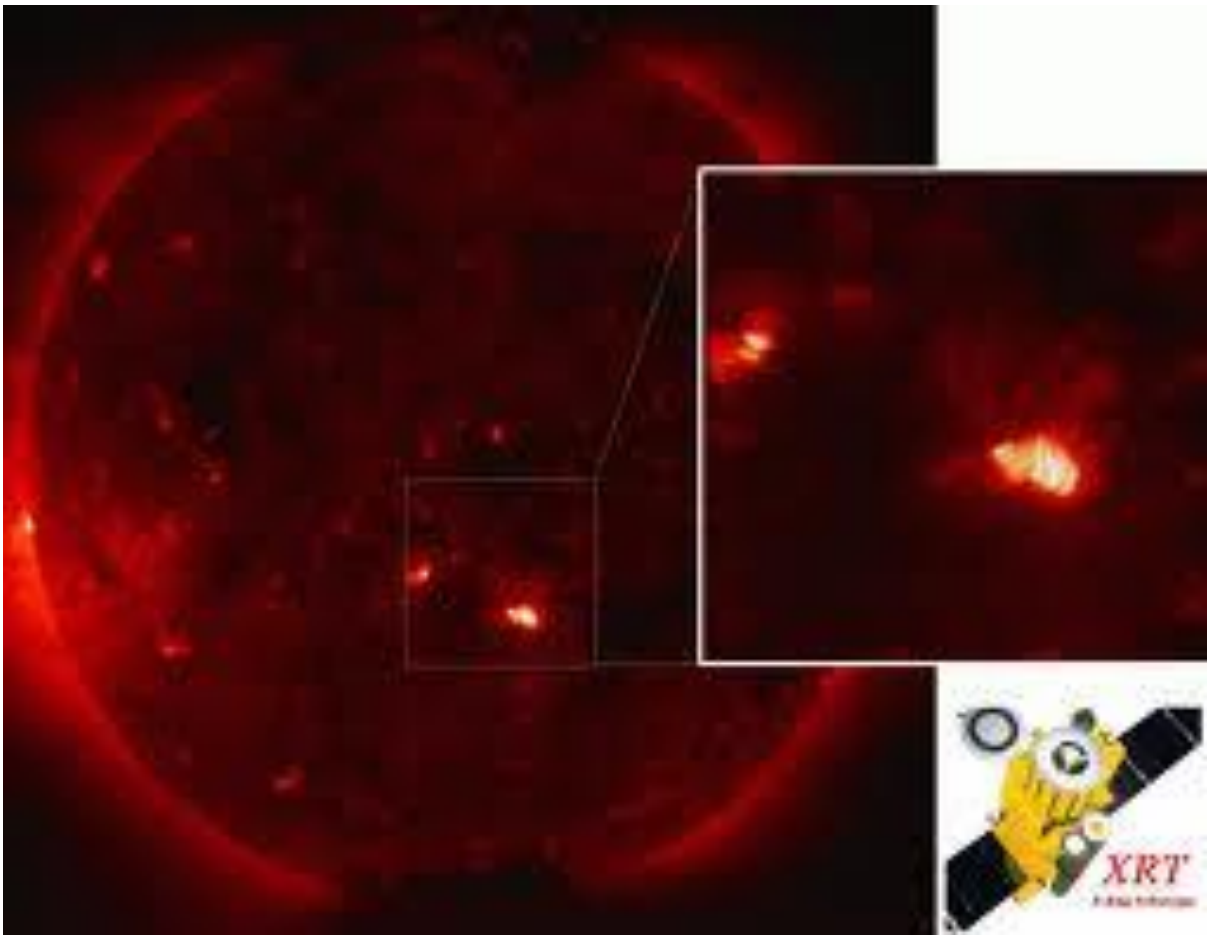

Figure 1.9

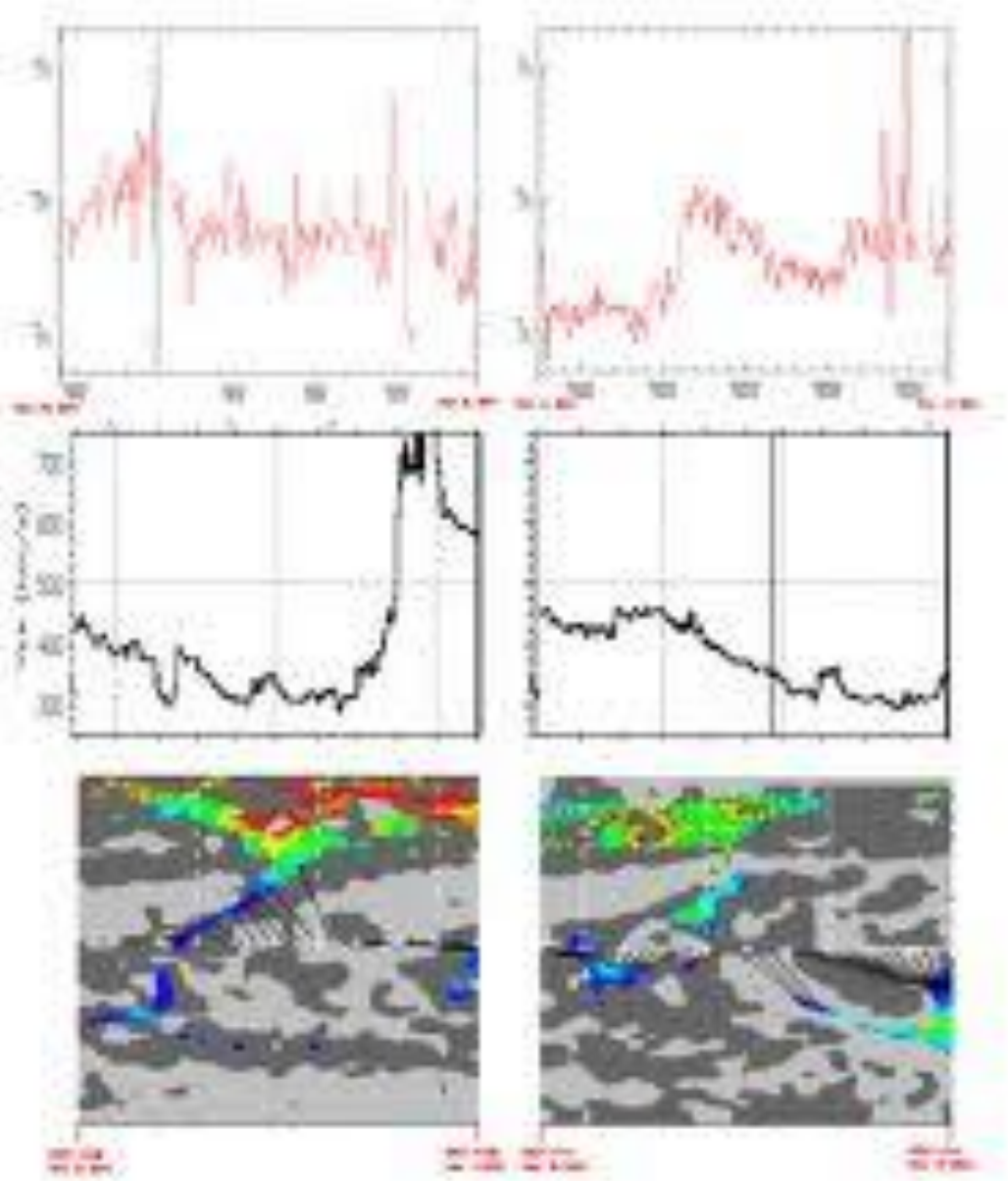

Figure 1.10

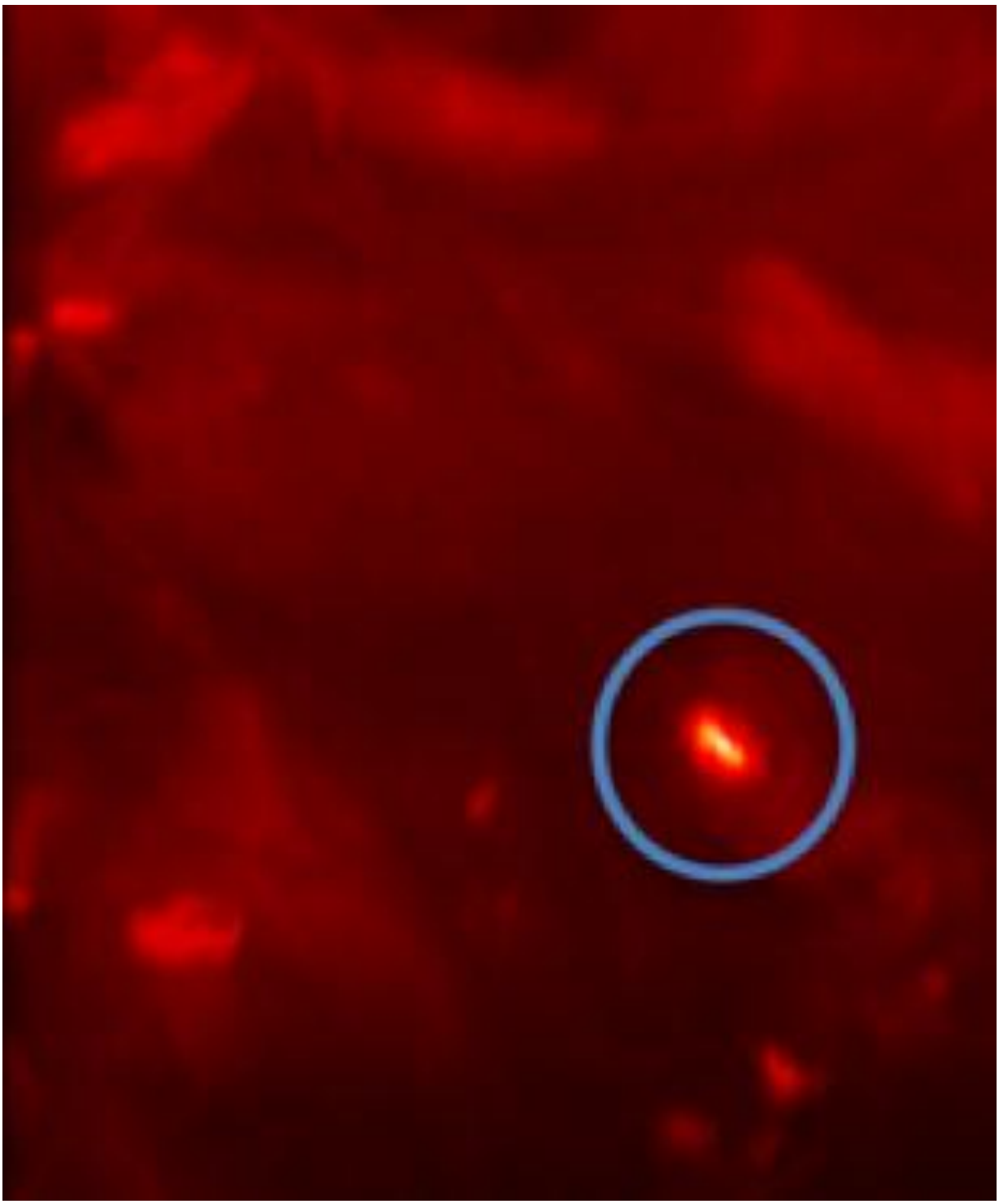

Figure 1.11

In these pictures (Figures 1.9,1.10,1.11) coronal bright points are shown clearly, bright and bigger coincide with their features. And their features are described in two axes in picture 1.10. On the other hand figure figure 1.9 and figure 1.11 illustrated coronal bright points clearly.

Another approach to dynamics of coronal bright points. The Sun Watcher using Active Pixel system detector and Image Processing (SWAP) onboard the PRoject for OnBoard Autonomy-2 (PROBA2) spacecraft provides images of the solar corona in EUV channel centered at 174 Å. These data, together with the Atmospheric Imaging Assembly (AIA) and the Helioseismic and Magnetic Imager (HMI) onboard Solar Dynamics Observatory (SDO), are used to study the dynamics of coronal bright points. The evolution of the magnetic polarities and associated changes in morphology are studied using magnetograms and multi-wavelength imaging. The morphology of the bright points seen in low-resolution SWAP images and high-resolution AIA images show different structures, whereas the intensity variations with time show similar trends in both SWAP 174 Å and AIA 171 Å channels. We observe that bright points are seen in EUV channels corresponding to a magnetic flux of the order of 1018 Mx. We find that there exists a good correlation between total emission from the bright point in several UV–EUV channels and total unsigned photospheric magnetic flux above certain thresholds. The bright points also show periodic brightenings, and we have attempted to find the oscillation periods in bright points and their connection to magnetic-flux changes. The observed periods are generally long ($10-25$ minutes) and there is an indication that the intensity oscillations may be generated by repeated magnetic reconnection.

CHAPTER 2. RESULTS OF STUDY CHARACTERISTICS AND EVOLUTION CORONAL BRIGHT POINTS

2.1. Observing point like features in extra ultraviolet

Three-dimensional Structure and Evolution of Extreme-ultraviolet Bright Points Observed by STEREO/SECCHI/EUVI

We unveil the three-dimensional structure of quiet-Sun EUV bright points and their temporal evolution by applying a triangulation method to time series of images taken by SECCHI/EUVI on board the STEREO twin spacecraft. For this study we examine the heights and lengths as the components of the three-dimensional structure of EUV bright points and their temporal evolutions. Among them we present three bright points which show three distinct changes in the height and length: decreasing, increasing, and steady. We show that the three distinct changes are consistent with the motions (converging, diverging, and shearing, respectively) of their photospheric magnetic flux concentrations. Both growth and shrinkage of the magnetic fluxes occur during their lifetimes and they are dominant in the initial and later phases, respectively. They are all multi-temperature loop systems which have hot loops (~106.2 K) overlying cooler ones (~106.0 K) with cool legs (~104.9 K) during their whole evolutionary histories. Our results imply that the multi-thermal loop system is a general character of EUV bright points. We conclude that EUV bright points are flaring loops formed by magnetic reconnection and their geometry may represent the reconnected magnetic field lines rather than the separator field lines.

Ultraviolet spectrograms and spectroheliograms of the solar chromosphere are used to test the suggestion (Dere et al. 1986, Rutten & Uitenbroek 1991a) that bright points observed at h = 1600 Å, chromospheric jets observed in CI lines near h = 1560 Å, and Ca II K2V bright points are associated with each other and that they are all manifestations of the same wave interaction

in the non-magnetic chromosphere. We search for spatio-temporal connections between 1600 Å bright points and CI blue jets using data from the HRTS VI rocket mission, comparing 1600 Å spectroheliograms and a co-spatial CI Dopplershift map on a pixel-by-pixel basis. We find no direct evidence for spatial co-location of bright points and jets, not for instantaneous correspondence and also not when allowing for phase delays as long as three minutes. Also, the average brightness evolution and its rms uctuation are not obviously different between sites of large CI blueshift and the remaining surface.

Another group of researchers have important role to develop that work and they wrote following sentences:

We measure the heights of EUV bright points (BPs) above the solar surface by applying a stereoscopic method to the data taken by the Solar TErrestrial RElations Observatory/SECCHI/Extreme UltraViolet Imager (EUVI). We have developed a three-dimensional reconstruction method for point-like features such as BPs using the simple principle that the position of a point in the three-dimensional space is specified as the intersection of two lines of sight. From a set of data consisting of EUVI 171 Å, 195 Å, 284 Å, and 304 Å images taken on 11 days arbitrarily selected during a period of 14 months, we have identified and analyzed 210 individual BPs that were visible on all four passband images and smaller than 30 Mm. The BPs seen in the 304 Å images have an average height of 4.4 Mm, and are often associated with the legs of coronal loops. In the 171 Å, 195 Å, and 284 Å images the BPs appear loop-shaped, and have average heights of 5.1, 6.7, and 6.1 Mm, respectively. Moreover, there is a tendency that overlying loops are filled with hotter plasmas. The average heights of BPs in 171 Å, 195 Å, and 284 Å passbands are roughly twice the corresponding average lengths. Our results support the notion that an EUV BP represents a system of small loops with temperature stratification like flaring loops, being consistent with the magnetic reconnection origin.

Connect of CBP with small scale magnetic field. Coronal bright points (CBP), point like bright features in solar corona, are observed over entire solar disc - in quiet and active regions, in coronal holes, etc., and present during all cycle – from solar minimum to solar maximum. As bright features in solar corona, CBP must be connected to solar magnetic fields. Previous studies of CBP and small scale magnetic fields (magnetic elements, ME) didn't answer to the question on connection of CBP and ME. Moreover, a latitudinal distribution of CBP differs from the one of ME. It is known that the magnetic fields of quiet and active regions are different. We study evolution of CBP in different regions of solar corona: in quiet and active region, and coronal holes. In this report the evolution of CBP in different regions of solar corona is presented. The mechanism of flaring of CBP is discussed.

Point like features, named X-ray bright points (XBP), were discovered on X-ray images of Sun obtained with sounding rocket in 1969 (Vaiana et al. 1970). Later on images of Sun in Extreme ultraviolet the point like features also were observed (Bruner et al. 1996, Zhang et al. 2001) and then the point like features in solar corona have got more common name as coronal bright points (CBP). Bipolar magnetic fields are associated with CBPs in the photosphere (Golub et al. 1977). The magnetic fields must have such area as CBP and oriented as CBP. Recently X-Ray telescope (XRT: Golub et al. 2007; Kano et al 2008) aboard the Hinode satellite (Kosugi et al. 2007) and Atmospheric Imaging Assembly (AIA) aboard SDO resolves XBP complex loop-like structures (Ueda et al. 2010, Li et al. 2012). It's supposed that the loop like structures give us to directly see coronal magnetic field configuration.

Ueda et al.(Ueda et al 2010) have found 24% of the XBPs are due to emerging bipoles, while remaining 76% are due to chance encounter of opposite polarities and an orientation distribution of XBP is similar to the distribution for the bipolar magnetic fields. The XBP orientation is, however, much more random than that of the bipolar magnetic fields with similar size. Li et all (Li et al. 2012) have found the magnetic bipoles associated with bright points at 1600

Å, the orientation angles are distributed randomly along the equator. Ueda et al. 2010 and Li et al. 2012 have studied CBP and bipoles (BP) the same area as CBP in the small quit region near the solar disk center and found that there are two types of XBP by place in solar magnetic fields: XBP is connected with emerging bipoles and they due to chance encounter of opposite polarities. We have divided CBP in two types by their maximal intensity, dim and bright, and founded that dim CBP are observed all over solar disk in the same time bright CBP- in the active region belts (Sattarov et al. 2010, 2011). In this paper we study orientation of CBP and small scale BP and the magnetic field configuration all over the corona by orientation of CBP and BP.

Rotation of Solar Corona from Tracking of Coronal Bright Points

1) Solar rotation. An automated procedure for identification of coronal bright points is applied to selected EIT images observed at various phases of the solar cycle. The procedure finds about 400 bright points on a single EIT image observed at 195 Å. The positions of the bright points are tracked to study the profile of solar rotation in the solar corona. It is shown that the rotation of coronal bright points closely follows the latitudinal rotation profile of the underlying photospheric magnetic field. It is also demonstrated that coronal features situated at the same heliographic coordinates but different heights in the corona may exhibit different rotation rates.

It is well established that at the photosphere and chromosphere the Sun rotates differentially: equatorial zones rotate faster than the polar regions. The latitudinal profiles of rotation vary slightly for different features; e.g., supergranules rotate faster than sunspots, and younger sunspots rotate faster than the older ones (for a recent review see Beck 2000). On the other hand, the differential rotation in the corona is not that profound (Howard 1984). Antonucci & Svalgaard (1974) studied the rotation of the green corona (Fe XIV 5303) for the years 1947–1970 and found an indication of differential rotation in some periods. In a follow-up study, Antonucci & Dodero (1977) found that the differential rotation in the corona is present at the maximum and the declining

phases of a sunspot cycle. Sime et al. (1989) showed that the coronal differential rotation is most profound at the late stages of the ascending phase of a solar cycle. More recently, Weber et al. (1997, 1999) employed data obtained by the Yohkoh Soft X-Ray Telescope (SXT) to study rotation rates of coronal holes, diffuse corona, and active regions during the declining phase of cycle 22 and rising phase of cycle 23. Figure 3 in Weber et al. (1997) and Figures 3 and 4 in Weber et al. (1999) indicate that the X-ray corona does not exhibit any significant differential rotation. On the other hand, Altrock (2003) analyzed synoptic observations of the green (Fe XIV 5303) and red (Fe X 6374) coronal lines from 1976 (Fe XIV) and 1983 (Fe X) to 2001 and found the presence of a weak, solar cycle dependent differential rotation in both spectral lines.

Previous studies of coronal rotation that employed the feature-tracking technique emphasized larger structures such as active regions and coronal holes. At the same time, some studies (Antonucci & Dodero 1977; Sime et al. 1989) clearly associate the presence of differential rotation with the presence of solar active regions on the disk. Coronal bright points (CBPs) offer an alternative feature that can be used to track solar rotation even during solar minimum, when no active regions are present. The lifetime of CBPs, ranging from about 2 to 48 hr (Golub et al. 1974, 1976), is adequate to determine the solar rotation with sufficient precision; CBPs are present at all latitudes, and their number varies inversely with sunspot cycle (Davis 1983; Sattarov et al. 2002; Hara & Nakakubo-Morimoto 2003). Since CBPs are present both inside and outside the coronal holes (CHs), they can be used to study the presence of differential rotation inside the CHs. Earlier studies (e.g., Timothy et al. 1975) indicated rigid rotation of coronal holes. Later studies showed that the magnetic field inside a CH may not follow the rigid rotation. It is still unknown how coronal features situated inside the coronal hole rotate with respect to the CH boundaries. Some models of CHs (e.g., Nash et al. 1988; Wang & Sheeley 1993, 2004) suggest that CHs maintain rigid rotation by "adjusting" their boundaries via reconnection with the outside magnetic field. Within the framework of these

models, coronal features inside CHs should not necessarily rotate as rigidly as the whole CH. Recently, Braja et al. (2002) used observations by the EUV Imaging Telescope (EIT) on the Solar and Heliospheric Observatory (SOHO) from 1998 June to 1999 May to study solar rotation in 284 Å data. Coronal bright points and other bright features were either manually identified or selected using the Regions of Interest Segmentation IDL program. The coordinates of the selected areas were used to determine the solar rotation. Braja et al. (2002) found differential rotation present in the data for the coronal bright points and small active regions. However, during 1998–1999 sunspot activity was high, so the presence of differential rotation in the corona might be attributed to the presence of sunspots (Antonucci & Dodero 1977).

In our study, we use coronal bright points to explore the presence of differential rotation during periods of low sunspot activity. We automatically identify coronal bright points using the data from SOHO EIT at 195 Å (Delaboudinière et al. 1995). A typical lifetime of coronal bright points is about 8 hr, and 195 Å data provide a much better time cadence (12 minutes) for tracking CBPs than 284 Å data with their 6 hr time cadence. Use of an automatic procedure eliminates subjective criteria from the CBP selection. Section 2 briefly describes our procedure of CBP identification. In § 3 the coordinates of selected bright points are used to determine the latitudinal profile of solar rotation during the period of deep solar minimum, and in § 4 we discuss our findings.

2) Data and procedure for coronal bright points identification.

In this work we use calibrated SOHO EIT images (264 pixel-1) observed at 195 Å during two periods of deep solar minimum (1996 April 16 and July 28). Both days were located in the middle of prolonged periods without sunspot activity. For comparison, we have also included observations on 2005 May 5–6, when the sunspot activity was low but not negligible.

To identify CBPs, we used the automatic procedure that we developed (Sattarov et al. 2005a, 2005b). The procedure was modified to improve

classification of some CBPs (showing variation in brightness) as either previously existing or newly emerged bright points. To identify CBPs, we first subtract a median-smoothed image from the original full-disk data. The size of the median filter was determined on the basis of comparison of CBPs selected by our program with CBPs selected using a fixed intensity threshold as in Zhang et al. (2001). For that part, the intensity threshold was computed as the averaged intensity plus three standard deviations over an area 150 × 150 in size centered at the solar disk center. When determining the size of the median filter, we used EIT observations for days with low sunspot activity near solar minimum in 1996. After subtracting the median-filter average, we compute the average brightness Iavg and its standard deviation using a difference image (with pixels corresponding to potential bright points and active regions excluded). According to Sattarov et al. (2005a), the distribution of intensity in each EIT image can be decomposed into two components: a Gaussian core corresponding to a diffuse quiet-Sun corona and a broad wing corresponding to an active corona. A brightness level Ithresh that separates these two components was adopted as the threshold of potential bright points or active regions. Pixels with intensity less than Ithresh (on the original image) were used to compute Iavg. Finally, potential CBPs were selected as features where the intensity exceeds the Icut = Iavg + 3 level on the difference image. The final selection of coronal bright points was accomplished using the total area of the potential CBPs, their shape, and their angular distance from the disk center (< 0.95 R). We excluded features whose radii were smaller than 2 Mm or larger than 20 Mm. We also excluded highly elongated and crescent-like structures reminiscent of a single bright loop. The criteria for minimum and maximum CBP radius are based on the results of a manual survey by Longcope et al. (2001).

Subtracting a median-filtered image from the original image improves the identification of bright points. Unfortunately, in some cases it might also lead to the false identification of bright portions of active region loops as coronal bright points. To prevent this from happening, Sattarov et al. (2005a)

excludes areas of active regions from consideration. On the other hand, we found that for the 1996 April–July data, large active region–like coronal structures were deselected on the basis of their size (radius larger than 20 Mm), and no additional active region masking was necessary.

Next, each selected coronal bright point was identified in all of the following images using two-dimensional cross-correlation. Cross-correlation was computed over a 50 pixel × 50 pixel window. CBPs for which the solar limb was within their cross-correlation windows were excluded. (This further limits the range of solar latitudes to approximately ±70° depending on the B0 angle.) The displacements determined from cross-correlation were used to study solar rotation in the corona at the height of formation of Fe XIV 195.3 Figure 1 shows examples of EIT images with all identified coronal bright points. Figure 1a also shows intensity contours that approximately mark the boundaries of coronal holes. The intensity level corresponding to CH boundaries was determined by visual comparison with the coronal hole boundaries from the National Solar Observatory (NSO) at Kitt Peak He 10830 observations.

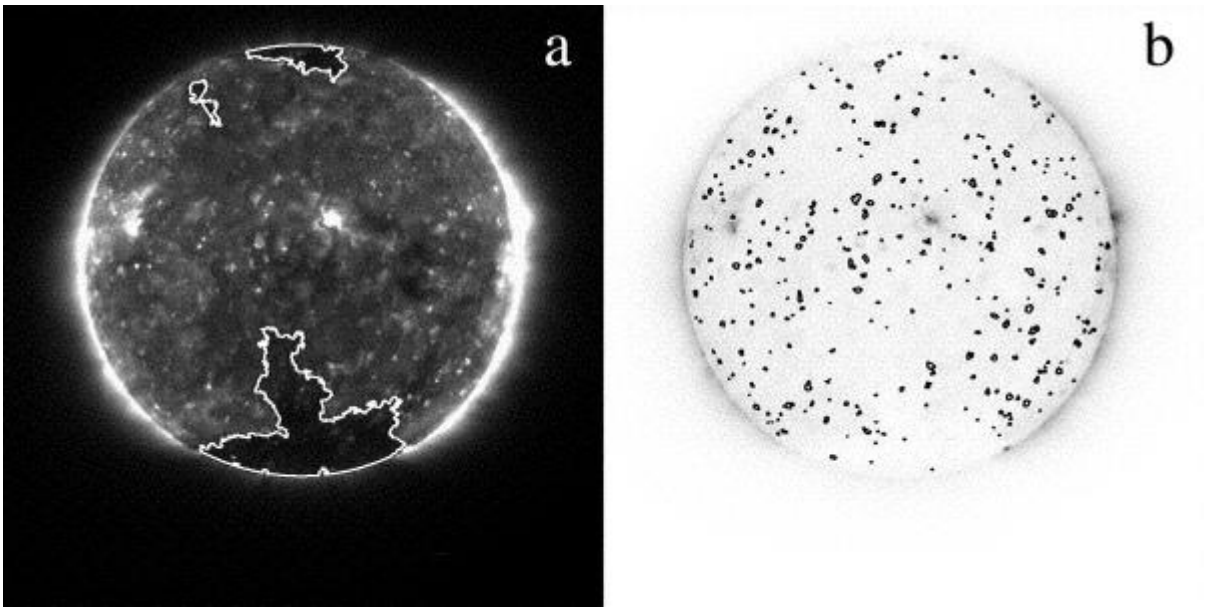

Fig. 2.1. Example of CBP selection. (a) EIT image observed on 1996 April 16 at 195 Å; contours show approximate boundaries of coronal holes. (b) Contours of CBPs selected by our automated procedure.

Golub et al. (1975) and later Sattarov et al. (2002) explained the bimodal latitudinal distribution of CBPs within a framework of two types of coronal

bright points associated with ephemeral active regions and canceling bipoles ("classical" CBPs). The existence of different types of coronal bright points was also suggested in several earlier studies (e.g., Harvey-Angle 1993). Webb et al. (1993) investigated the correspondence between X-ray bright points (XBPs) and magnetic features and concluded that the majority of XBPs are associated with canceling magnetic features (MFs). A small fraction of XBPs were found to be associated with old ephemeral active regions, and almost no XBPs were associated with young ephemeral regions. Figures 2.1 shows examples of both types of bright points. CBPs associated with the ephemeral regions exhibit behavior reminiscent of an emerging bipolar magnetic structure (small active region), while classical CBPs do not exhibit significant evolution in their magnetic and coronal structure. However, this study does not separate coronal bright points by their type because of an insufficient number of Michelson Doppler Imager (MDI) full-disk magnetograms during 1996 April–July.

Fig.2.2 Coronal bright point (left column, at the center of image) associated with an ephemeral active region–type growing magnetic bipole (right column) on 1996 April 16 at (a) 00:48 UT, (b) 04:16 UT, (c) 05:23 UT, (d)

10:11 UT, (e) 15:09 UT, and (f) 14:59 UT.

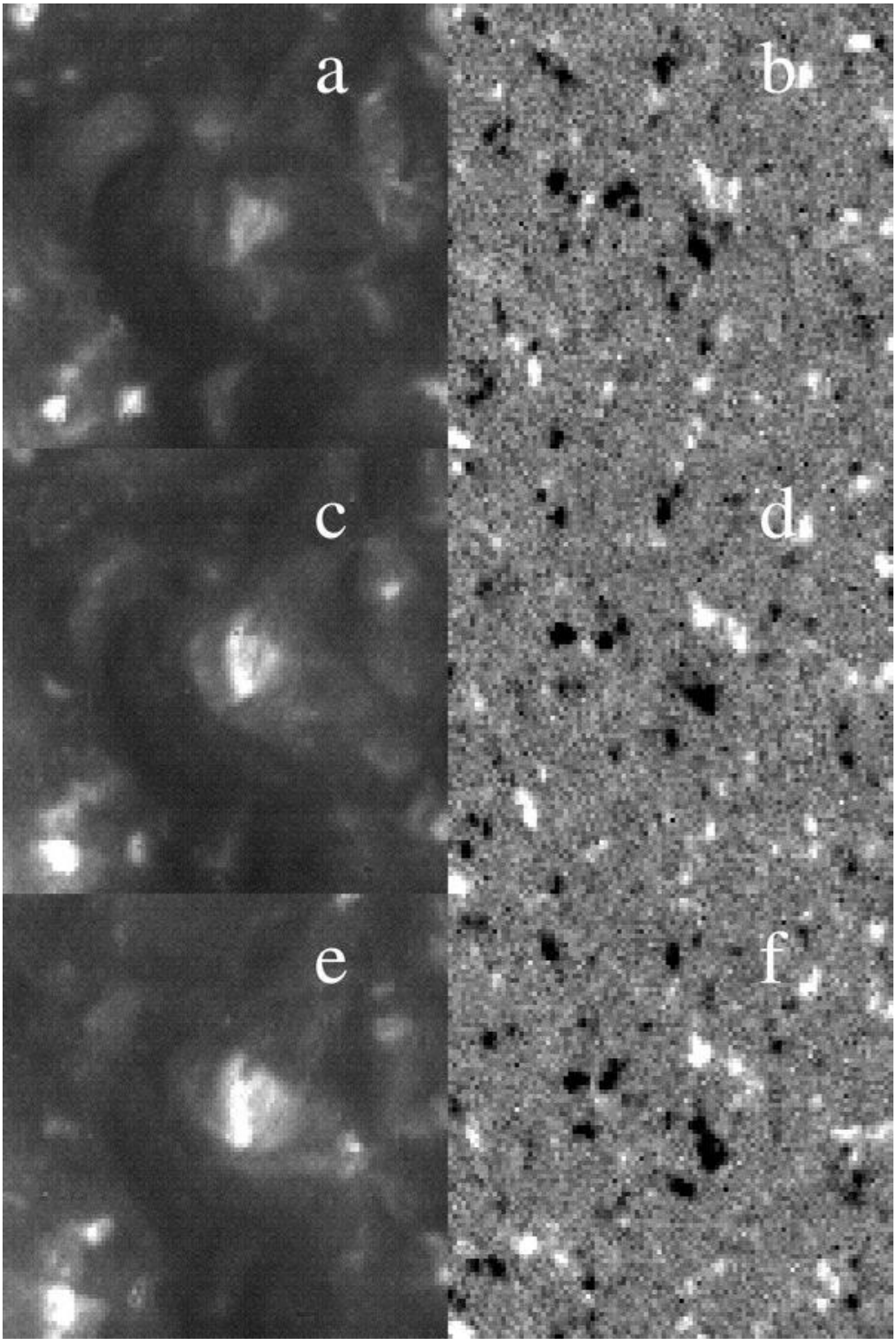

Figure 2.2

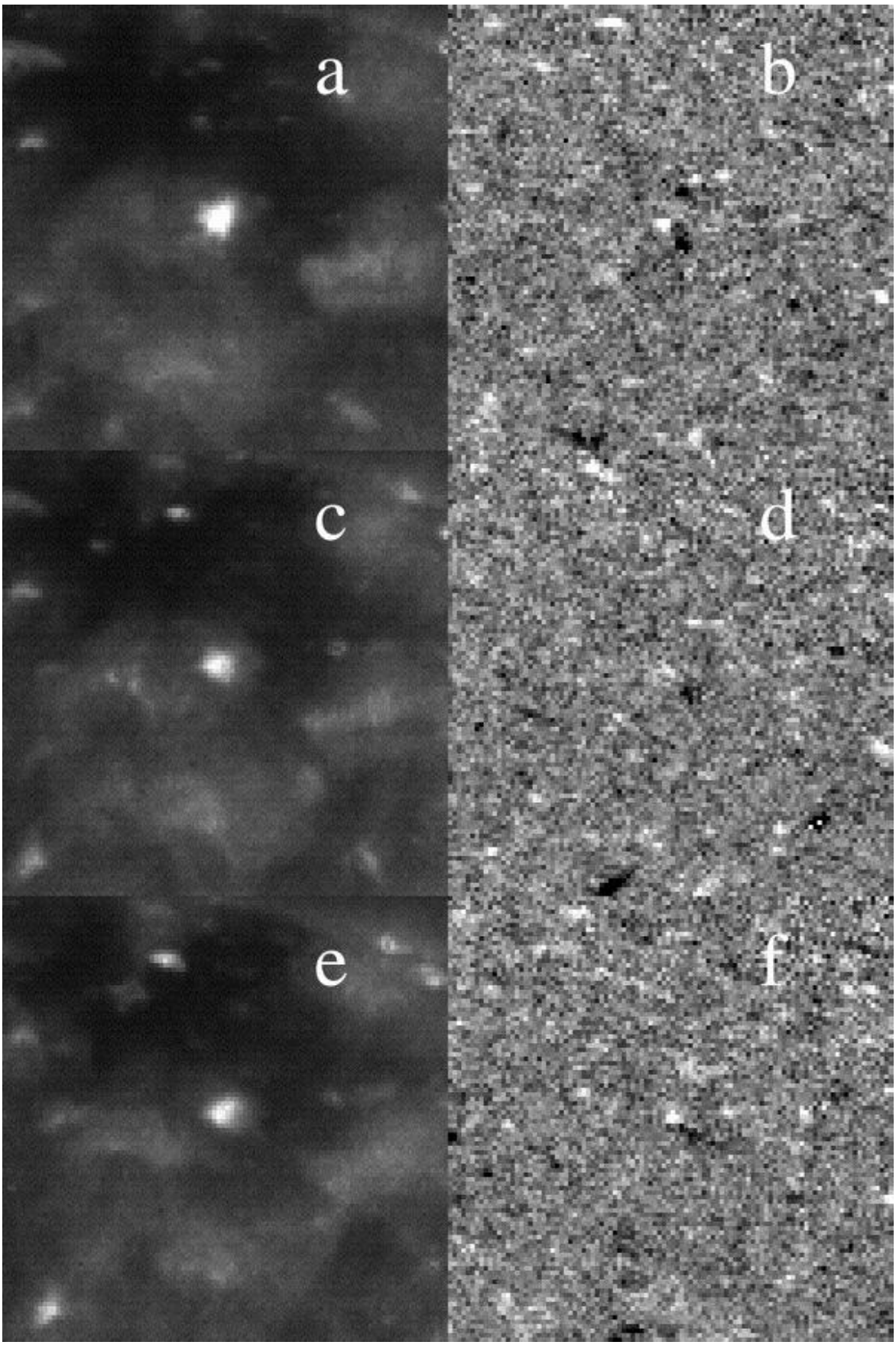

Fig.2.3. Coronal bright point of the classical type associated with a canceling bipole on 1996 April 16 at (a) 04:06 UT, (b) 05:23 UT, (c) 06:19 UT, (d) 10:11 UT, (e) 08:33 UT, and (f) 14:59 UT. 3 Fe XIV 195 forms at a height

of 80,000 km (Zhang et al. 2000). Braja et al. (2004), however, estimated the height of bright points observed in 284 Å at 8000–12,000 km.

3) Latitudinal Rotation Profiles. After identifying each coronal bright point on all sequential images, we determined their heliographic coordinates (latitude and central meridian distance [CMD]). The change in CMD with time was approximated by a first-degree polynomial, and the slope of the approximation was used to represent the daily rotation rate of this CBP. Only CBPs that were present in at least five consecutive images were selected for this determination. To minimize projection effects, only CBPs within ±45° of the central meridian were included in determination of the rotation rate. Figure 2.4 shows profiles of solar rotation for all three periods (1996 April 16, July 28, and 2005 May 5–6).

Fig.2.4. Sidereal rotation profiles of coronal bright points (dots) for three periods: (a) 1996 April 16, (b) 1996 July 28, and (c) 2005 May 5–6. Open circles indicate CBPs situated inside coronal holes. In panel (c) squares and asterisks correspond to the western and eastern boundaries of the coronal hole, respectively. Solid curves show a second-degree polynomial fit to the data. The dashed curve is a parabolic approximation of the rotation of the coronal hole boundaries.

Despite significant scatter, solar differential rotation is present in all three periods. The scatter in Figure 2.4 can be attributed to evolution and proper motions of some bright points, as well as errors in displacements determined using two-dimensional cross-correlation.

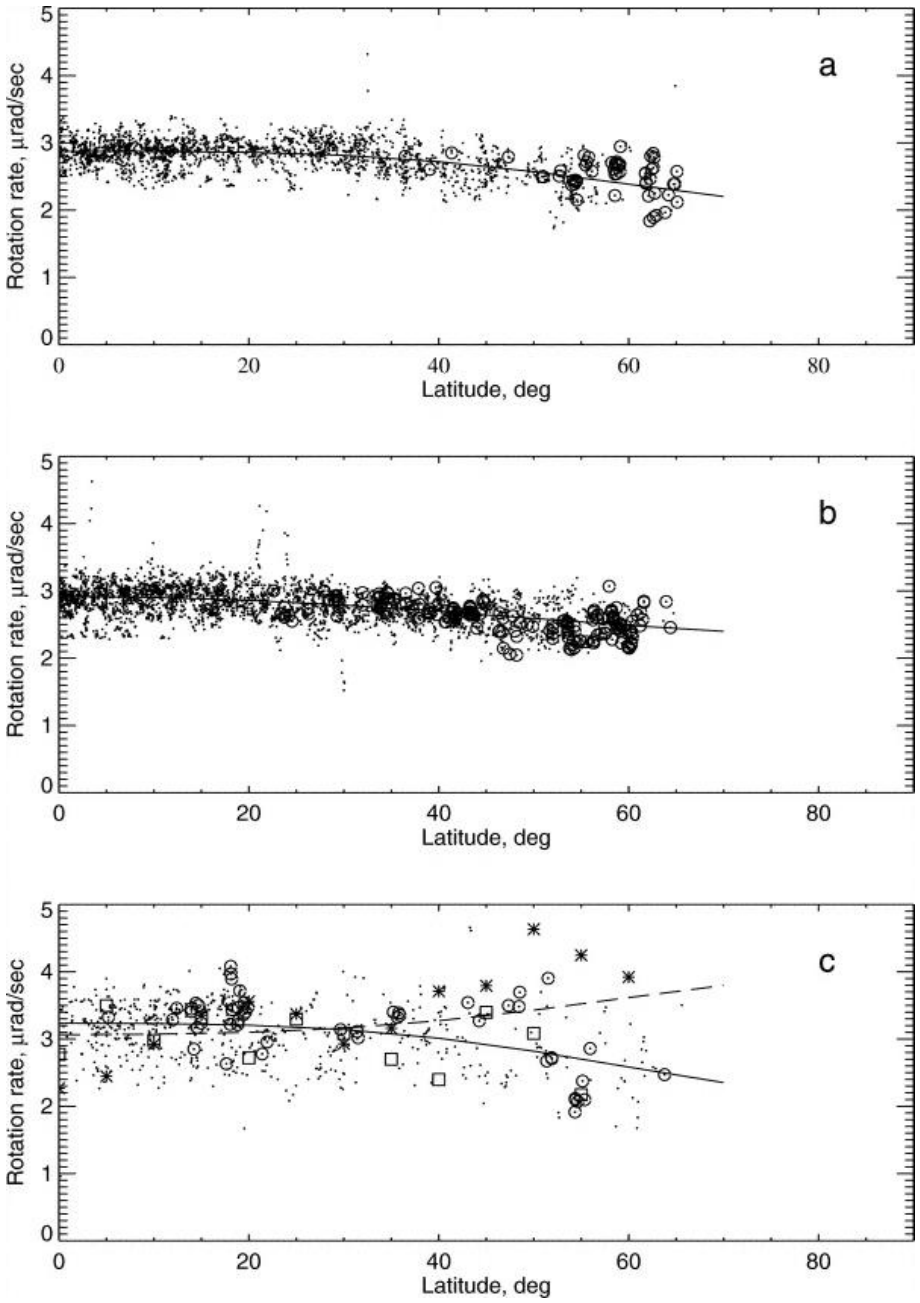

Figure 2.4

In general, the CBPs' latitudinal profile of solar rotation is similar to the active regions' profile. For comparison with previous studies of solar rotation, we fit the data by A + B + C , where is the solar latitude and the coefficients A, B, and C are listed in Table 1. The coefficients of the above approximation are in general agreement with previous studies (e.g., see summaries by Howard [1984] and Beck [2000]) with an equatorial rotation rate of about 142–145 day-1. The equatorial rotation rate on 2005 May 5–6 is higher than in the 1996 April 16 and July 28 data (solar minimum).

Table 1 Sidereal Solar Rotation Profiles.

Data	A ($^{\mu}$rad s^{-1})	B ($^{\mu}$rad s^{-1})	C ($^{\mu}$rad s^{-1})
1996 Apr 16...	2.875 ± 0.007	-0.032 ± 0.066	-0.827 ± 0.102
1996 Jul 28...	2.919 ± 0.006	-0.495 ± 0.061	-0.106 ± 0.096
2005 May 5–6...	3.235 ± 0.025	-0.132 ± 0.257	-0.983 ± 0.381

On 1996 April 16 and July 28, three high-latitude CHs were present. On 2005 May 5–6, a large coronal hole extended across the disk from the north pole to the equator. We drew the boundaries of the CHs on the EIT 195 Å images using a fixed intensity threshold. The threshold was determined by visual comparison with the published coronal hole boundaries from the NSO Kitt Peak He I 10830 data. Comparing the rotation rates of CBPs situated inside and outside the CHs, we found no systematic difference between the two. Within the uncertainties of the data, CBPs inside the coronal holes follow the same latitudinal profile of solar rotation as the CBPs situated outside the CHs.

In addition to the CBPs' rotation rates, we have also measured the rotation rate of the coronal hole boundaries. Points of intersection between the boundaries of the CHs (threshold level) and fixed latitudes were tracked to determine the rotation rate of the western and eastern boundaries of the CH on 2005 May 5–6. However, due to the complicated boundaries of the CHs at high latitudes, we were unable to measure the rotation rates of the CHs in the 1996 April 16 and July 28 images using this method. The eastern and western boundaries of the coronal hole observed on 2005 May 5–6 rotate with different rates (Fig. 4c). At low latitudes, the eastern boundary of this CH rotates faster than the western boundary, and at high latitudes, the western boundary rotates faster. The difference in the rotation rates of the two boundaries implies that this CH decreases in size at low latitudes and grows at high latitudes. However, the average rotation rate of the two boundaries is nearly constant at low to middle (0°–50°) latitudes (see the parabolic approximation; Fig. 4c, dashed curve). The increase in the rotation rate of this CH at high latitudes implied by the parabolic approximation can be attributed to the lack of data points for the eastern

boundary. Thus, on average, this CH rotates rigidly at low to middle latitudes. Coronal bright points situated inside this CH rotate with a broad range of velocities within the rotation rates of the two CH boundaries. Despite significant scatter, CBPs inside the coronal hole do follow the same profile of differential rotation as the CBPs situated outside the CH

2.2. Connection of CBP with small scale magnetic field (BP)

1. Data Sets and Automatic Procedure for Identification and orientation of CBP and small scale magnetic bipoles

In this work we use full disk images observed by the Extreme-ultraviolet Imaging Telescope (EIT, Delaboudinière *et al.*, 1995) on board of SOHO. We utilize EIT full disk synoptic data with spatial resolution of 2.64 arcsec per pixel and six hours cadence observed in 195 Å from 1996 – 2012. The data are calibrated following the standard EIT data reduction routine. The calibration routine normalizes the exposure time and takes into account change in response of CCD camera over the time of mission. The automatic procedure identified CBP and determinate heliographic coordinates, maximal intensity, area and orientation (tilt) of the CBP (Sattarov et al. 2010). Method define of orientation is the same as in Ueda et al. (Ueda et al. 2012). Using the National Solar Observatory (NSO) at Kitt Peak full disk longitudinal magnetograms (SOLIS) and at a different (G) threshold for magnetic fluxes, we have identified a small scale BP from 2003 – 2012 and determined their orientation (tilt) to solar equator. Procedure of identification BP was described in Sattarov et al. (Sattarov et al. 2002) and BP's orientation determining is added to the procedure. The procedure fixes large and small axes of CBP (if CBP hasn't cycle form) and finds angle (θ) between the large axis and solar equator as it is described in Ueda et al. (Ueda et al. 2010). The procedure finds also error of the angle ($\Delta\theta$).

2. Data analyses

The Automatic Procedure used in this study identifies CBP with area from 2 up to 286 pixels (sizes 5- 50 arcsec). The total number of CBPs at solar minimum is about 600 and at solar maximum – 450 per image. For this study we used CBP with the error ($\Delta\theta$) less than _____. Figure 2.5 shows the histogram of distribution of CBP (separately for dim and bright) along the orientation angle (tilt) for a) 1996 and 2007-2008 (solar minimums), b) 2000-2003 (solar maximum). The left histogram for solar minimum is in general similarly but right one is differ to the histogram obtained by

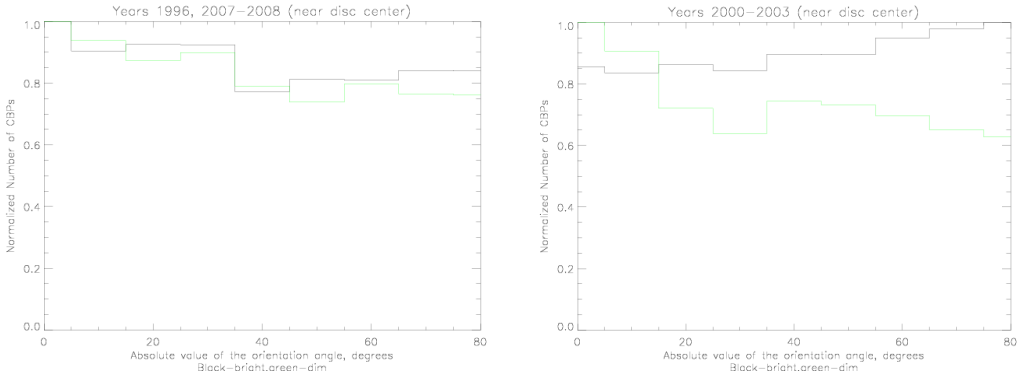

Figure 2.5. Histogram of distribution CBP (black – bright and green - dim) along orientation to solar equator (tilt): a) solar minimum, b) solar maximum.

(Fig. 2.5(7) in Ueda et al. 2010). At solar minimum both, bright and dim CBPs are oriented along solar equator, whereas at maximum bright CBPs has more along meridian orientation than dim one's. This is first differing between two types CBP (Sattarov et al. 2010).

It was found (Sattarov et al. 2007, 2010) the latitudinal distribution of dim CBP uniformly over solar globe and circumscribe by cosine of latitude, whereas the one of bright CBP at solar maximum has two humped curve as number of sunspot. It seems the small scale bipoles emerge at active region belts and the bright CBP connected with the bipoles. Figure 2.6 reproduces the histogram of number of bipoles at different flux by the orientation to solar equator (tilt). At large angles the number is low for bipoles with flux low then 10 gauss and high for bipoles with flux more then 15 gauss.

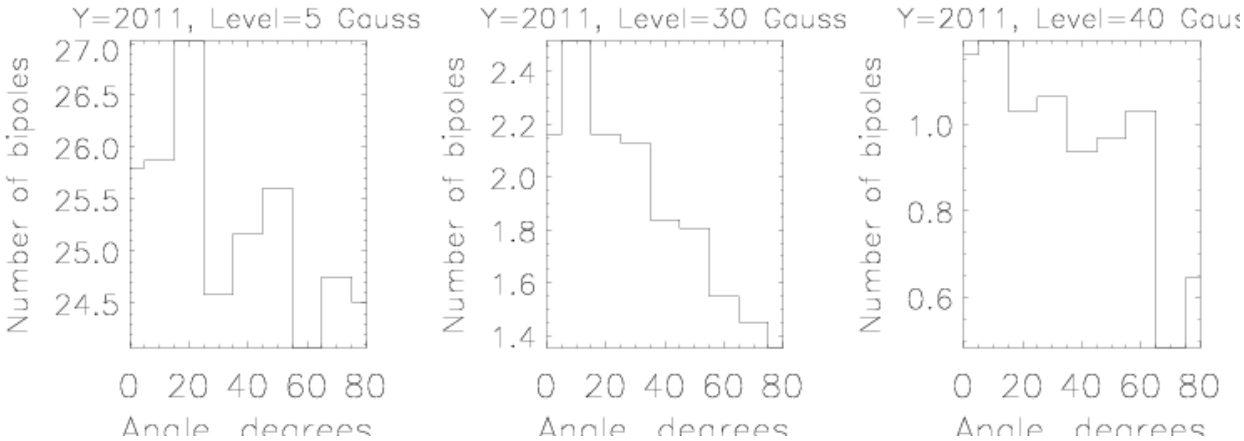

Figure 2.6. Histogram of number of small scale bipoles at different flux by angle of its axes to solar equator.

2.3. Cycle variation of CBP

It was described an automatic routine to identify coronal bright points (CBPs) and apply this routine to SOHO/EIT observations taken in the 195 Å spectral range during solar cycle 23. We examine the total number of CBPs and its change in the course of this solar cycle. Unlike some other recent studies, we do find a modest ≈30% decrease in the number of CBPs associated with maximum of sunspot activity. Using the maximum brightness of CBPs as a criterion, we separate them on two categories: dim CBPs, associated with areas of a quiet Sun, and bright CBPs, associated with an active Sun. We find that the number of dim coronal bright points decreases at the maximum of sunspot cycle, while the number of bright CBPs increases. The latitudinal distributions suggest that dim CBPs are distributed uniformly over the solar disk. Active Sun CBPs exhibit a well-defined two-hump latitudinal profile suggestive of enhanced production of this type of CBPs in sunspot activity belts. Finally, we investigate the relative role of two mechanisms in cycle variations of CBP number, and conclude that a change in fraction of solar surface occupied by the quiet Sun's

magnetic field is the primary cause, with the visibility effect playing a secondary role.

Cycle time variation is a metric and philosophy for continuous improvement with the aim of driving down the deviations in the time it takes to produce successive units on a production line. It supports organizations' application of lean manufacturing or lean production by eliminating wasteful expenditure of resources. It is distinguished from some of the more common applications by its different focus of creating a structure for progressively reducing the sources of internal variation that leads to workarounds and disruption causing these wastes to accumulate in the first place. Although it is often used as an indicator of lean progress, its use promotes a structured approach to reducing disruption that impacts efficiency, quality, and value.

Solar cycle 23 in Coronal Bright Points

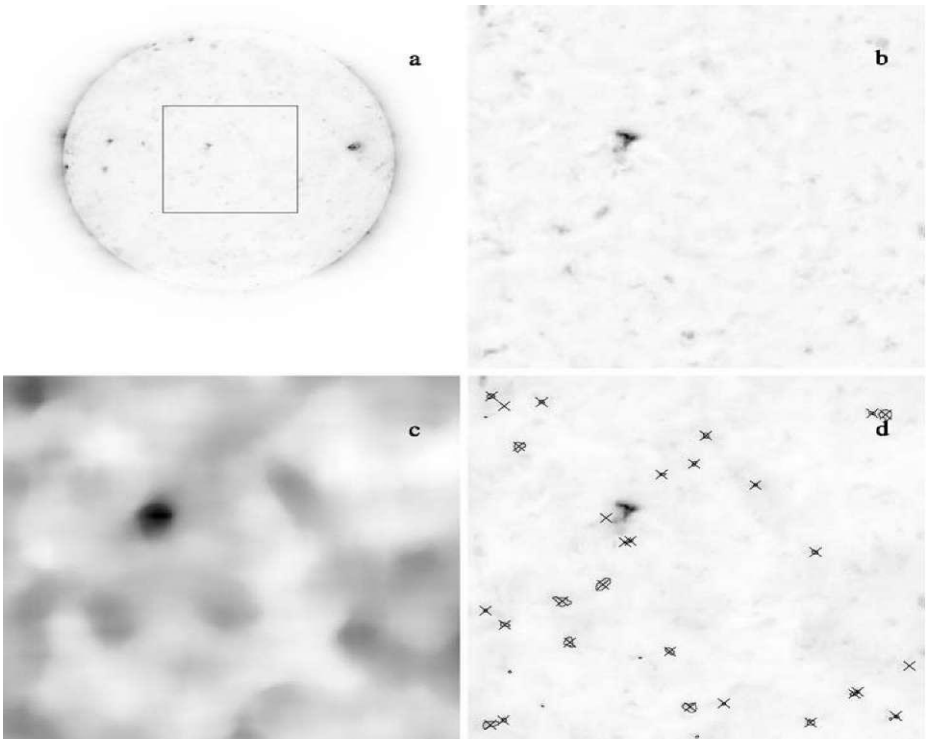

Figure 2.7. EIT full disk image (reversed colors) taken on 2 April 1996. For demonstration purposes, panel (b) shows an area of 300 pixels by 300 pixels near disk center, the same area smoothed by median filter (c), and coronal bright points selected using the fixed intensity threshold (contours) and by our method (crosses). Note that the brightest feature on panel (d) did not pass the "active region" threshold and, hence, is not selected as a CBP.

Figure 2.7. EIT full disk image (reversed colors) taken on 2 April 1996. For demonstration purposes, panel (b) shows an area of 300 pixels by 300 pixels near disk center, the same area smoothed by median filter (c), and coronal bright points selected using the fixed intensity threshold (contours) and by our method (crosses). Note that the brightest feature on panel (d) did not pass the "active region" threshold and, hence, is not selected as a CBP.

Figure 2.8 shows the monthly-averaged number of coronal bright points per solar visible disk during 1996 - 2008. The CBP number exhibits a clear decrease associated with a maximum of the sunspot activity cycle; this decrease is at odds with some previous studies of coronal bright points. For example, data due to McIntosh and Gurman (2005) show an unexplained jump in CBP number in early 1998 as well as a slight increase towards 2002, a year on he sunspot cycle maximum. On the other hand, Hara and Nakakubo-Morimoto (2003) have found a small (~ 20%) increase in the total number of X-ray bright points associated with the minimum of solar cycle 22.

The total number of CBPs in our data set is about 280-450 per image, which exceeds the number of bright points found in McIntosh and Gurman (2005) for Fe XIII 195 A (230 - 300)

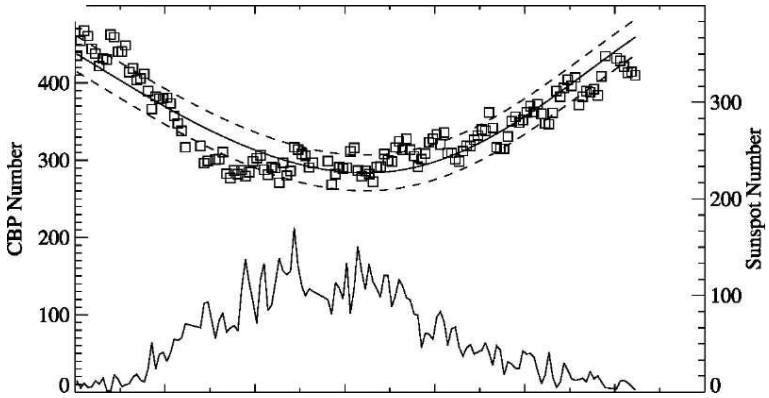

Figure 2.8 Cycle variation of coronal bright points (monthly-averaged, squares) and monthly sunspot number (lower curve). The solid line surrounded by two dashed lines represents the change in CBP number with solar cycle derived on the basis of a Gaussian fit to the distribution of dim and bright CBPs shown in Figure 2.10. The two dashed lines represent one sigma standard deviation of the fit shown by the solid line.

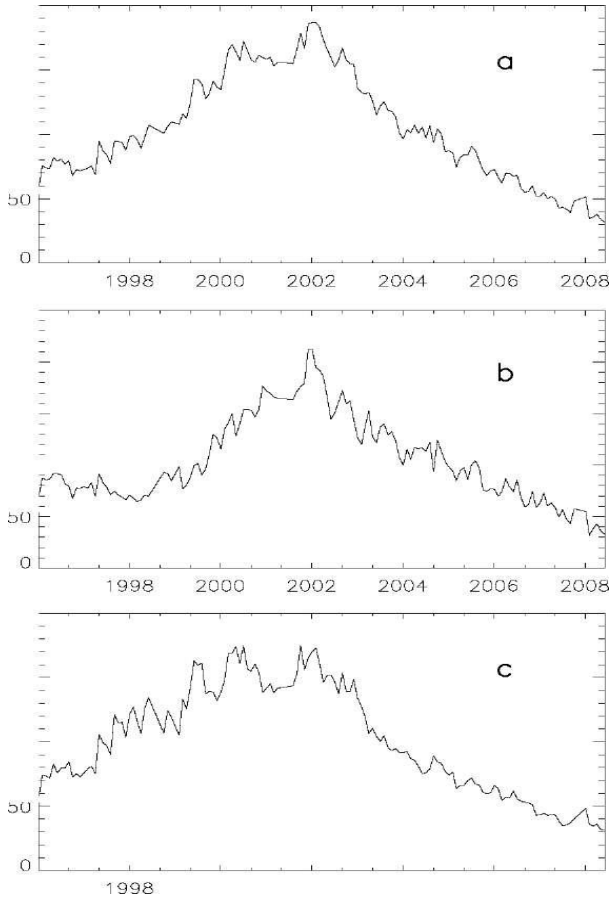

Figure 2.9 Cycle variation of background intensity for: (a) full disk, (b) equatorial region (latitudinal range 0 ± 5 degrees), (c) active region belts (+20 ± 5 degrees and -20 ± 5 degrees), and (d) high latitudes (+50 ± 5 degrees and -50 ± 5 degrees). It is the direct effect of bright active regions, whose presence may increase the brightness of a diffuse corona even at a significant distance away from an active region *(e.g.,* Pevtsov and Acton, 2001). At the rising phase of cycle 23, when the decaying fields of sunspots of cycle 22 were still present near the equator, we see an enhanced coronal brightness both at mid-latitudes (Figure 2.9c) and near the equator (Figure 2.9.b). As the cycle progresses and the sunspot activity drifts to low latitudes, we see a sharper decrease in coronal

brightness in mid-latitudes and a more gradual decrease near the equator. This behavior supports our interpretation of active regions as the source of an enhanced corona in the vicinity of CBPs.

It is interesting to note that our CBP identification routine appears to be relatively insensitive to changes in the sensitivity of the EIT detectors. For example, a drastic change in quantum efficiency of EIT CCD in 1997 - 1999 did not result in a significant change in background intensity (see Figure 4) or total number of CBPs (Figure 2.8) The EIT response graph indicates that between 1996 and 1997, the detector's response for Fe XII 195 A had decreased by 50%. Despite this drastic change, however, the CBP number remains nearly constant (Figure 2.8). Between 1999 and 2008, the detector's response had gradually decreased from 80% (of pre-launch value) to about 15%. Contrary to that, however, Figure 2.8 shows a gradual increase (not decrease) in CBP numbers during same period. To further evaluate the effects of changes in the detector's response, we have conducted the following experiment. We have selected a typical EIT image and reduced its overall intensity by 50%. Because CCD is a linear detector, one should expect that a loss of sensitivity will have a linear effect with respect to the image brightness. The total number of CBPs for this degraded image is only about 10% smaller as compared with the original image. To simulate a non-linear change in the CCD response, we reduced the contrast of our test image by 10%. This resulted in only a minor reduction (about 1%) of the total number of CBPs as compared with the original image. Thus, we believe that a change in the EIT detector's response over the lifetime of the SOHO Mission does not have a significant effect on the CBP number returned by our routine.

In addition to the enhanced background surrounding CBPs, we also see cycle-related variations in maximum brightness of CBPs (not shown). The average CBPs brightness is higher near the maximum of sunspot cycle, and it is lower during the sunspot minima. The enhanced brightness of CBPs near the maximum of a sunspot cycle may indicate the presence of an additional

population of bright points associated with stronger fields of active regions. The presence of two populations of CBPs was previously suggested by several researchers. To investigate the cycle behavior of two CBP populations, we have divided our data set into two categories: dim CBPs with maximum intensity $/_{max}$ < 150 DNs^{-1} and bright CBPs with $/_{max}$ > 150 DNs^{-1}. The maximum brightness threshold, $/_{max}$ = 150 DNs^{-1}, was selected on the basis of the variation of $/_{max}$ during solar cycle. Thus, for example, in 1996, when the sunspot activity was extremely low, the maximum CBP intensity peaked at about 150 DNs^{-1} (see Figure 2.9.), which we have adopted as a threshold for dim CBPs.

Figure 2.10 shows the cycle variation of two types of CBPs. The number of dim CBPs decreases as the sunspot activity grows, while the number of bright CBPs increases. A similar behavior of bright and dim CBPs with solar cycle was previously reported by Hara and Nakakubo-Morimoto (2003). The numbers of dim (N_{dim}) and bright (N_{bright}) CBPs show a linear relation, albeit with a

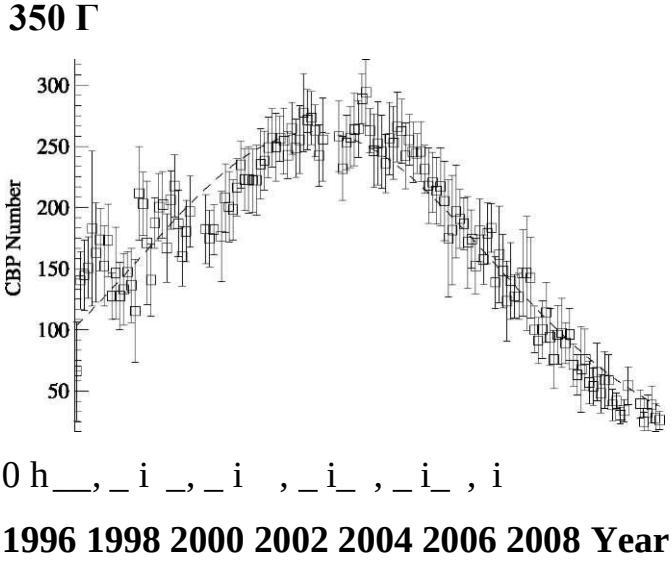

significant scatter. By fitting the first degree polynomial, we found that N_{bright} = (274 ± 4) - (0.59 ± 0.02)N_{dim}. The proportionality coefficient being less than unity suggests that an increase in the number of bright CBPs cannot not fully compensate for a decrease in the number of dim CBPs, and hence, one could expect to find a slight decrease in the total number of CBPs at/near maximum of sunspot activity.

Figure 2.10 (a) shows a Gaussian fit to distributions of dim and bright CBPs with solar cycle. A sum of these two Gaussian fits is shown as a solid line in Figure 3; two dashed lines correspond to a standard deviation of this fit. The trend suggests a solar-cycle variation of total CBP number at about 30% level. The trend is statistically significant, well exceeding the scatter in data points in Figure 3.

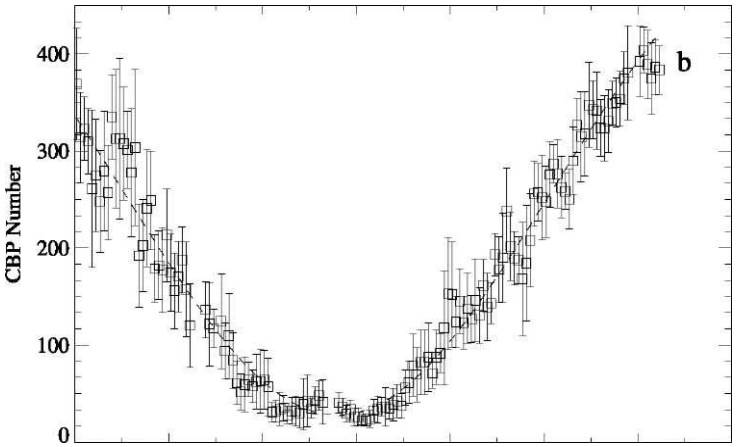

Figure 2.10 (b) Cycle variation of (a) "bright" and (b) "dim" CBPs. Open squares with error bars show monthly-averaged numbers of CBPs and their standard deviations. Dashed lines are approximations of two distributions by Gaussian functions.

The above relation between number of bright and dim CBPs provides an indirect support to early findings by Webb *et al.* (1993) and Harvey-Angle (1993) who showed that a majority of CBP are associated with canceling bipoles and about one third of them are associated with ephemeral active regions. Assuming that dim CBPs are primarily associated with quiet Sun bipoles, and bright CBPs are "active Sun" features, one can arrive to the conclusion that overall the quiet Sun features well-outnumber the active Sun CBPs. The latitudinal distribution of two types of CBPs is also different. Dim CBPs are distributed more or less uniformly with solar latitudes (Figure 2.11, year 1996). The latitudinal profile of bright CBPs exhibits a well-defined hump during years when the sunspot activity is concentrated at mid-latitudes. The

latitudinal distribution of bright CBPs shows the migration toward the equator. When the activity belts migrate to the equatorial region, a two-hump pattern in the latitudinal distribution of CBPs disappears (Figure 2.12).

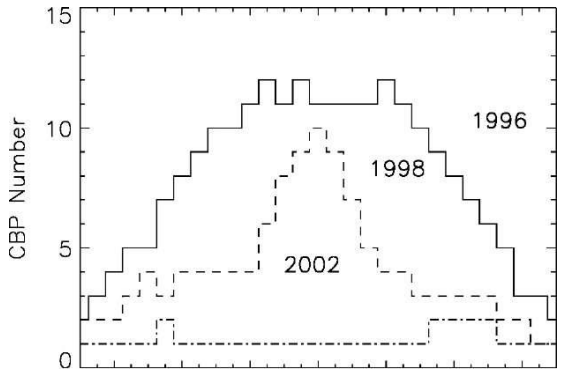

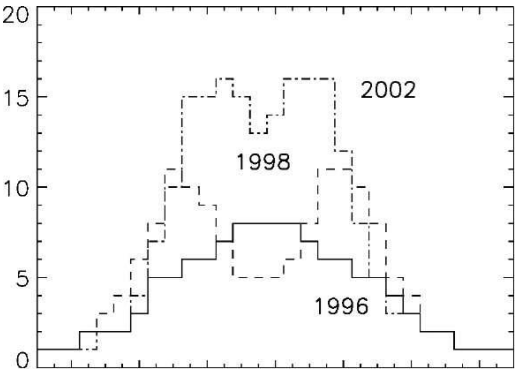

Figure 2.11 Figure 2.12

Figure 2.11 Average latitudinal profiles of number of "dim" CBPs for the years 1996 (solid), 1998 (dashed), and 2002 (dashed-dotted).

Figure 2.12 Average latitudinal profiles of number of "bright" CBPs for the years 1996 (solid), 1998 (dashed), and 2002 (dashed-dotted).

We would like to clarify, however, that our method separates coronal bright points into two types based on their brightness alone. It does not take into account the magnetic properties of CBPs, and therefore, we cannot be certain whatever "quiet Sun" CBPs are indeed associated with canceling bipoles in quiet Sun, nor can we state that "active Sun" CBPs are a product of ephemeral active regions. We plan to investigate such associations in a separate study.

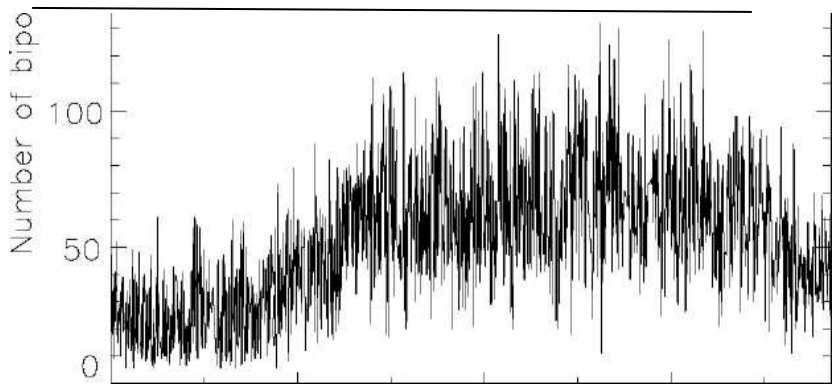

Figure 2.13 does not establish a causal relation between CBPs and magnetic bipoles. The question of a CBP-bipole association will be investigated separately.

Figure 2.13 Cycle variation of number of magnetic bipoles with unsigned magnetic flux larger than 50 G.

CHAPTER 3. MECHANISM OF FLARING CBP

3.1. Distribution of CBP on solar large scale magnetic field

Figure 3.1 shows Wilcox synoptic maps for CR 2055 (solar minimum) and 2120 (solar maximum) with orientation of axes CBPs at solar central meridian on it as shot dashes (hyphen), separately for dim (red) and bright (green) CBP. Apparently CBPs at high latitudes (more than 30 degrees) are oriented more along solar equator in the same times near solar equator they are oriented randomly.

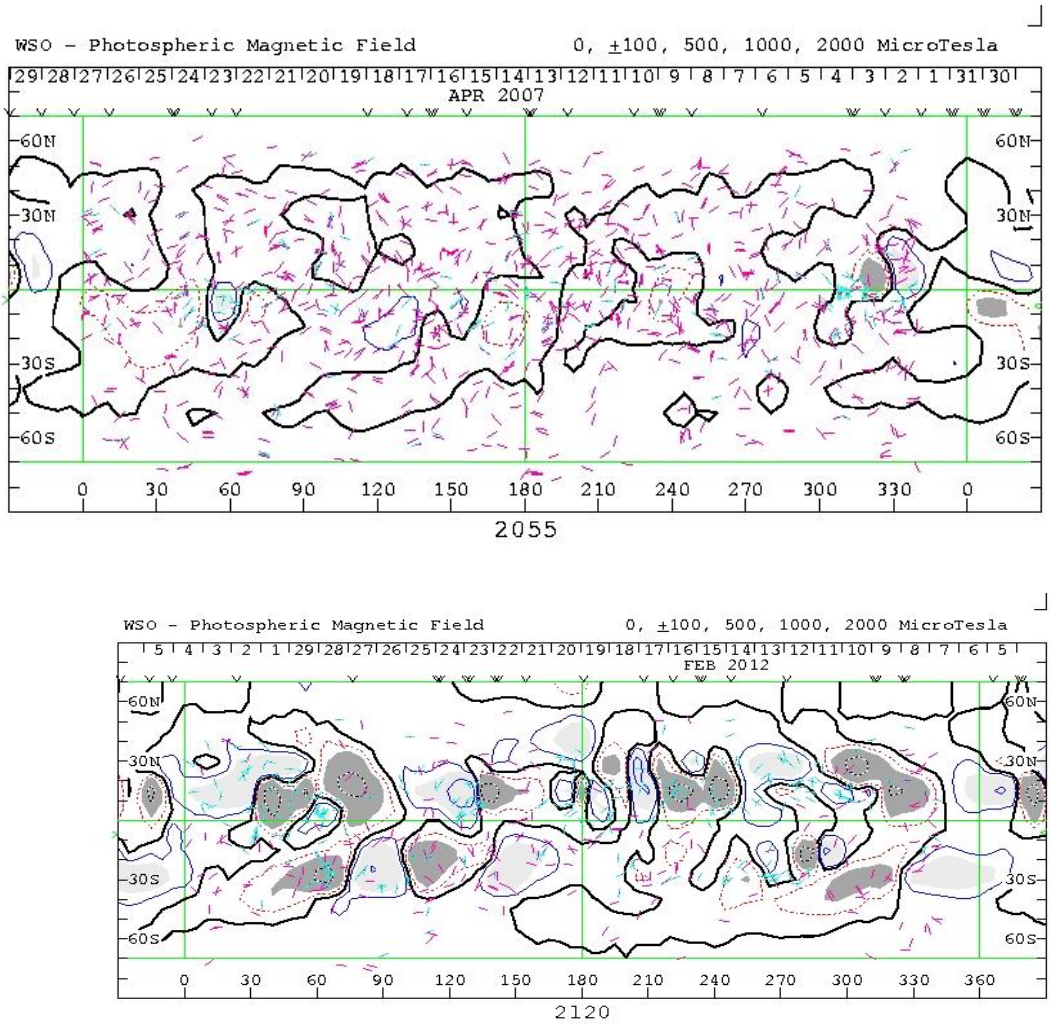

Figure 3.1. Wilcox synoptic maps CR2055 and 2120 with orientation of axes CBPs as short dashes (hyphen) on it (red-dim and green bright CBP).

Wilcox synoptic map is gotten as result of averaging-out of photospheres magnetic fields and presents solar large scale magnetic field.

At solar minimum coronal magnetic fields, as large scale magnetic field, taken out from photospheres one's by averaging, has more simple ordering and why both type of CBP oriented similarly (Fig. 1a and 3a). At solar maximum the field has simple ordering at high latitudes (Fig.3b) and the orientation of CBPs axes (Fig.1a) and low intensity bipoles (Fig.2a) also more ordering. In the same time the magnetic fields in active regions belts are more complicated, why CBP axes (Fig.1b) and high intensity bipoles (Fig.2c) in these regions are more randomly.

At last solar minimum (2008) our automatic procedure for identification has found approximately 600 dim and no one or small bright CBP. At now time (2012) half of all CBP was dim others bright. As it was found Ueda et al. (Ueda et al 2010) approximately a quarter of CBP connected with small scale emerging magnetic fields (BP) so at 2012 number of CBP connected with emerging BPs, bright ones by our definition, must be 75 and then the BPs has intensity about 25 gauss in chromospheres line 854.2 nm. At the same time dim CBPs are connected with BP of intensity a few gauss. It seems the high intensity bipoles and connected with them CBP are presented small scale emerging flux regions.

Sattarov et al. have found the bright CBPs correlated and dim one's anticorrelated with sunspot cycle. Recently Jin et al. (Jin et al. 2011) have found number of low (10^{19} Mx) flux magnetic elements anticorrelated and high (10^{20} Mx) one's correlated with sunspot cycle. Thus results received in this paper confirm conclusion obtained in Jin et al. 2011 and there are two types of coronal bright points which are formed by small scale magnetic fields (BP) different intensity. Orientation of axes (tilt) of low intensity BP and dim CBP is parallel to solar equator and high intensity BP and bright CBP are directed randomly. Orientation of axes of low intensity BP and dim CBP satisfied and high intensity BP and bright CBP are unavailable.

3.2. Connection between CBP and BP

Flares take place in active regions and provoke a sudden increase of the radiative flux emitted from small regions of the corona. They are very complex phenomena, visible at different wavelengths; they interest several zones of the solar atmosphere and involve many physical effects, thermal and not thermal, and sometimes wide reconnections of the magnetic field lines with material expulsion.Flares are impulsive phenomena, of average duration of 15 minutes, even if the most energetic events can last several hours. Flares involve a high and rapid increase of the density and temperature.

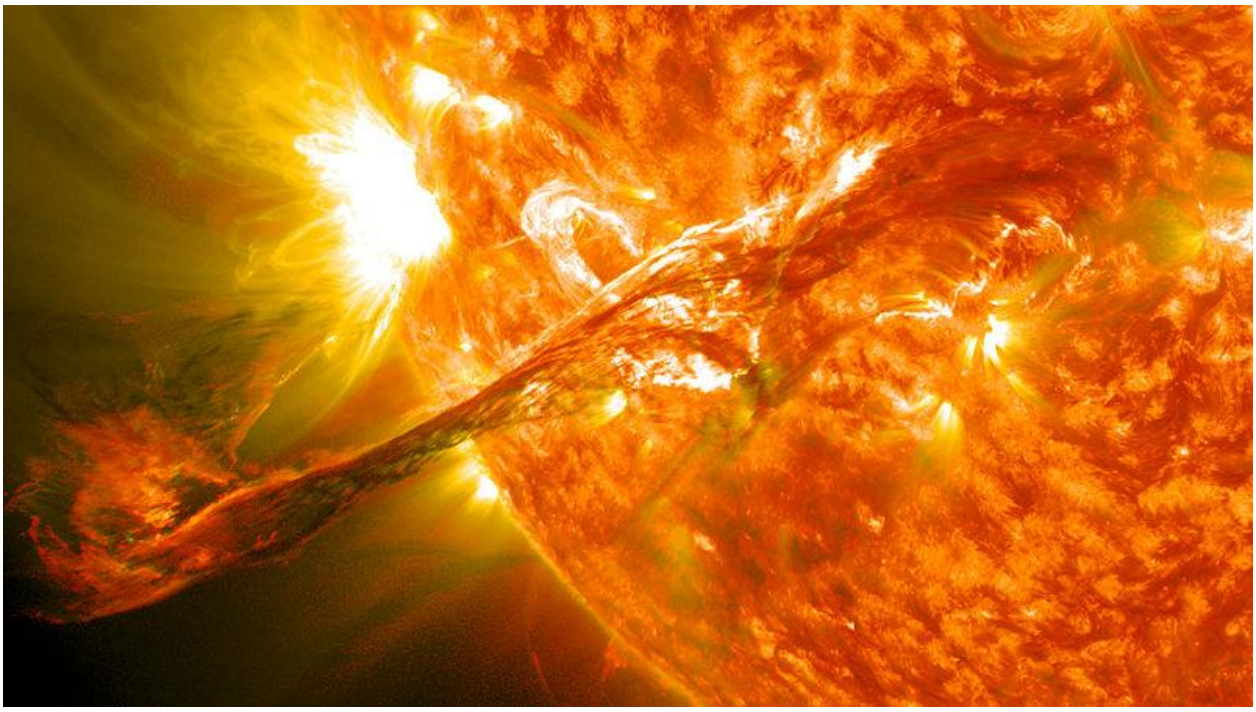

Figure 3.2 reveals a long filament of solar material that had been hovering in the Sun's atmosphere, the Corona, erupted out into space On August 31, 2012 at 4:36 p.m. EDT

An emission in white light is only seldom observed: usually, flares are only seen at EUV wavelengths and in the X-rays, typical of the chromospheric and coronal emission. In the corona the morphology of flares, which can be grasped from the observations in the soft and hard X-rays, at the UV wavelengths and in Hα, is very complex. However, two kinds of basic structures can be distinguished:

● Compact flares, when each of the two arches where the event is happening maintains its morphology: only an increase of the emission is observed without significant structural variations. The emitted energy is of the order of 1022 – 1023 J.

● Flares of long duration, associated to eruptions of prominences, transients in white light and two-ribbon flares: in this case the magnetic loops change their configuration during the event. The energies emitted during these flares of such large proportions can reach 1025 J.Filament erupting during a solar flare, seen at EUV wavelengths (TRACE)

As for temporal dynamics, three different phases are generally distinguished, whose duration are not comparable. These times, moreover, can depend on the range of wavelengths used to observe the event even considerably:

● an initial impulsive phase, whose duration is of the order of minutes. Strong emissions of energy are often observed even in the microwaves, at EUV wavelengths and in the hard X-rays.

● a maximum phase

● a decay phase, which can last several hours.

Sometimes also a phase preceding the flare can be observed, usually called as "pre-flare" phase.

This paper presents the formation, evolution and decay of a coronal bright point via a spectroscopic analysis of its transition region counterpart and the evolution of the underlying magnetic bipole during 3 days of almost continuous observations. The data were obtained with various instruments on-board SoHO, including the SUMER spectrograph in the transition region line S VI 933.40 Å, CDS in the He I 584.33, O V 629.73 and Mg IX 368.06 Å lines, plus MDI and EIT. The existence of the coronal feature is strongly correlated with the evolution of the underlying bipolar region. The lifetime of the bright point from the moment when it was first visible in the EIT images until its complete disappearance was ~ 18 hrs. Furthermore, the bright point only became

visible at coronal temperatures when the two converging opposite magnetic polarities were ~ 7000 km apart. As far as the temporal coverage of the data permits, we found that the bright point disappeared at coronal temperatures after a full cancellation of one of the magnetic polarities. The spectroscopic analysis reveals the presence of small-scale (~ 6′′) transient brightenings within the bright point with a periodicity of ~6 min. The Doppler shift in the bright point was found to be in the range of -10 to 10 km s^{-1} although it is dominated by a red-shifted emission which is associated with regions characterized by stronger "quiet" Sun photospheric magnetic flux. Small-scale brightenings within the bright point show velocity variations in the range 3-6 . In general the bright point has a radiance ~4 times higher than that of the network. No relation was found between the bright point and the UV explosive event phenomena.

Two-dimensional numerical magnetohydrodynamic simulations of a cancelling magnetic feature (CMF) and the associated coronal X-ray bright point (XBP) are presented. Coronal magnetic reconnection is found to produce the Ohmic heating required for a coronal XBP. During the BP phase where reconnection occurs above the base, about 90–95 per cent of the magnetic flux of the converging magnetic bipole cancels at the base. The last ≈5 to 10 per cent of the base magnetic flux is cancelled when reconnection occurs at the base. Reconnection happens in a time-dependent way in response to the imposed converging footpoint motions. A potential field model gives a good first approximation to the qualitative behaviour of the system, but the magnetohydrodynamics (MHD) experiments reveal several quantitative differences: for example, the effects of plasma inertia and a pressure build-up in-between the converging bipole are to delay the onset of coronal reconnection above the base and to lower the maximum X-point height.

Observations have revealed that the temperature of the quiet-Sun corona is maintained at a level of over a million degrees Kelvin, even though at solar minimum there are usually weeks without any large-scale coronal events such as solar flares or coronal mass ejections. Thus, it is likely that the many small-scale

events in the quiet-Sun corona (such as bright points, microflares and nanoflares) provide almost all the heat (e.g. Parnell & Jupp 2000; Parnell & Galsgaard 2004). The small-scale coronal magnetic field has a complex structure, where photospheric magnetic fragments of opposite polarity have multiple connections (e.g. Brown et al. 1999; Beveridge, Priest & Brown 2002; Beveridge, Longcope & Priest 2003; Close et al. 2004). These magnetic sources are in restless motion, fragmenting and merging, while new flux is continually emerging and old flux is cancelling. Consequently, this should lead to continual widespread magnetic reconnection and subsequent local heating throughout the whole corona, even when the Sun is quiet (Priest, Heyvaerts & Title 2002; Priest, Longcope & Titov 2003; Priest, Longcope & Heyvaerts 2005). Indeed, it has been found recently from observations that the coronal flux recycling time (which is the time it takes to reconnect all the coronal flux) is only at most 1.5 h in the quiet-Sun corona (Close et al. 2004), which is around 1/10 of the photospheric flux recycling time (Hagenaar 2001).

One type of observed small-scale heating phenomenon, which is associated with small-scale magnetic bipoles, is coronal X-ray bright points (XBPs), which are spread over all latitudes and longitudes of the low quiet-Sun corona (Golub et al. 1974). Coronal XBPs have been observed to release energies ranging from 1027 to 1029 erg. These values are based on the heating rates due to BPs observed by Habbal & Withbroe (1981), which range between 3 × 1023 and 1024 erg s−1, and on the lifetimes of BPs observed by Golub, Krieger & Vaiana (1976), which range between 2 and 48 h with an average of about 8 h. The rate of occurrence of XBPs over the whole quiet Sun is ≈5 × 104 per day if caused by small-scale bipoles of emerging flux [so-called ephemeral regions (ERs)] and ≈105 per day if caused by small-scale bipoles of cancelling flux [so-called cancelling magnetic features (CMFs); Martin, Livi & Wang 1985]. (For more details see von Rekowski, Parnell & Priest 2006, hereafter referred to as vRPP06.) Taking an energy release of 2 × 1027 erg per XBP, this results in a total heating rate from XBPs due to both ERs and CMFs of about 3 ×

1032 erg per day on the whole quiet Sun, that is, ≈6 × 104 erg cm−2 s−1. This energy gain rate from XBPs is about 20 per cent of the energy loss rate in the quiet-Sun corona, which Withbroe & Noyes (1977) reported to be 3 × 105 erg cm−2 s−1.

As mentioned above, around two thirds of coronal XBPs are caused by CMFs (e.g. Harvey 1985). Flux cancellation is the mutual loss of flux in equal proportions from each polarity (plus and minus). In an XBP event, possibly more than one photospheric filament of each polarity is interacting, as can also be the case in a cancellation event. CMFs involve flux convergence (Livi, Wang & Martin 1985) and flux submergence (Harvey et al. 1999), and significant downflows can be present (Chae, Moon & Pevtsov 2004). Martin et al. (1985) reported observations of total cancellation times of 1–24 h. Cancellation, coronal reconnection and coronal heating through XBP formation are linked, and studying these processes is important for solving the coronal heating problem.

Theoretical models of XBPs associated with CMFs have been developed in two and three dimensions by, for example, Priest, Parnell & Martin (1994), Parnell, Priest & Golub (1994a); Parnell, Priest & Titov (1994b), Parnell & Priest (1995), Longcope (1998), Longcope & Kankelborg (1999). Using three-dimensional (3D) magnetohydrodynamics (MHD) simulations, qualitative numerical studies of XBPs due to converging magnetic flux events have been made by, for example, Dreher, Birk & Neukirch (1997) and Neukirch, Dreher & Birk (1997). Quantitative numerical studies of CMFs and the associated XBPs are presented by vRPP06, using 2D MHD simulations. Building on the numerical model developed by Rickard & Priest (1994), vRPP06 were able to run their MHD experiments until cancellation was completed, in contrast to Rickard & Priest (1994). The initial magnetic configuration in vRPP06 has bipolar sources that are partially connected in such a way that the opposite-polarity sources marginally touch at the base. For this paper, we have developed a model where we start with a completely disconnected inner bipole, as is the case in the theoretical models of Priest et al. (1994) and Parnell et al. (1994a,b).

Thus, our simulations include both a complete CMF event and also a complete associated coronal XBP. Furthermore, we consider also unequal sources where the sources of the inner bipole have the same size and total flux, but a different flux distribution and hence a different maximum field strength. We compare our dynamically computed magnetic field configurations with the potential fields calculated from the converging sources at the base.

In both potential and numerical models, there is an overlying coronal field (which is created by flux connecting two outer sources of opposite polarity), and inner magnetic bipolar sources are moved towards each other by a horizontal flow at the base. This flow mimics footpoint motions and is the driver of the system, triggering cancellation and coronal reconnection and hence also creating the heating.

Coronal magnetic field, The time-evolution of the coronal magnetic field is shown in Fig. 4 for the potential field run DisEqNoPot, and for the corresponding MHD field run, namely DisEqNo0.01. We first describe the potential field evolution. In the first phase, before an X-point is created, the completely disconnected inner sources are advected towards each other. An X-point forms at the base at time $t \approx 200$, after which the inner sources become connected by Bx; at this time each of the two inner sources has been advected at the base over a distance of less than one source width so that the inner bipole is still separated at the base by more than two source widths. In the second phase, the X-point rises into the corona until time $t \approx 400$, when the base separation width is less than two source widths, and then moves back towards the base. During this coronal X-point phase there is coronal reconnection: field lines connecting inner and outer sources on each side of the axis reconnect around the X-point, adding flux to the field connecting the inner sources, as well as to the overlying field. This coronal magnetic reconnection, driven by converging sources, causes significant thermal energy release due to Ohmic heating, that is, a BP (cf. Section 3.3). These first and second phases are similar to those of Priest et al. (1994) in the coronal domain.

Figure 3.3

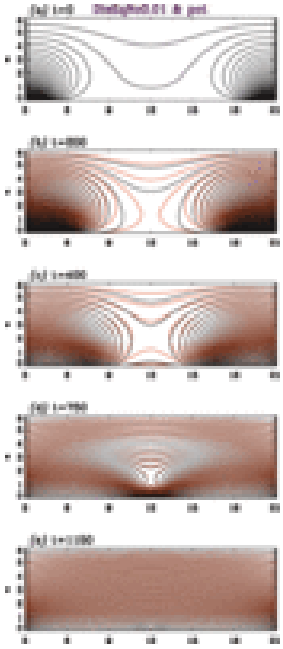

Coronal magnetic field evolution in the potential field model DisEqNoPot (orange/grey lines) and in the corresponding MHD field model DisEqNo0.01 (black lines). In the potential field evolution, the advection phase lasts until time t≈ 200, when an X-point forms at the base; the coronal X-point phase lasts from t≈ 200 until t≈ 1150, with the maximum X-point height at time t≈ 400. At time t≈ 1150, the X-point is back on the base in both models. The outer sources are not shown. Looking now also at the MHD field evolution, Fig. 3.3 shows that the creation of an X-point is delayed in the MHD case compared to the potential case.

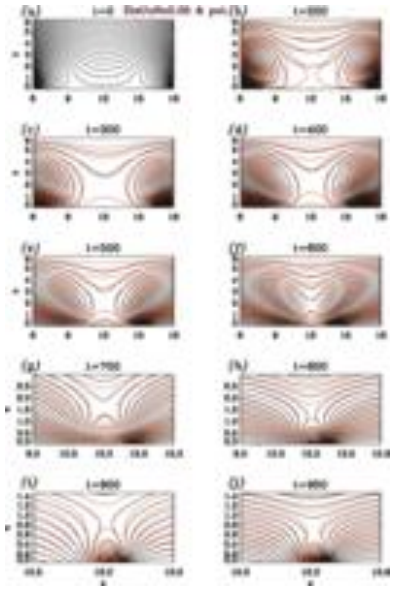

Magnetic field lines in Experiment DisUnNo0.05 with udriver= 0.05 at various times (black lines) and magnetic field lines for potential fields for comparison (orange/grey lines; Experiment DisUnNoPot), shown up to times where they differ noticeably. The times are rescaled to the case with udriver= 0.01, that is, multiplied by five. Note the repeated zooming-in in the last two panel rows.

Figure 3.4

When the top boundary is open to flow (see Fig. 3.5), the density build-up at the top boundary around the axis is less strong. This is partly due to an outflow developing in this region (with $u_z|_{top,axis} \leq 0.009$). The other reason is that matter is distributed along the outer overlying field by flows: a diverging horizontal flow is created along major parts of the top boundary (with $|u_x|_{top}| \leq 0.05$), and inflows form at the top close to the left and right boundaries (with

$u_z|_{top} \geq -0.0165$). (Note that the differences between Figs 3.4 and 3.5 are better visible in the colour version.)

Figure 3.5

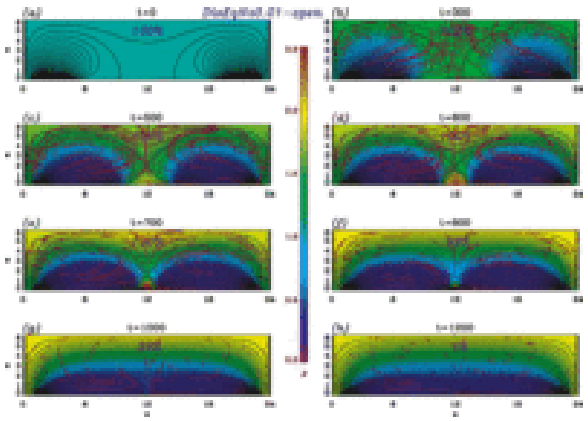

Same as in Fig. 3.4 but for Experiment DisEqNo0.01-open where the top boundary is open to flow.

The current density in Experiment DisEqNo0.01 is displayed in Fig. 3.6. First of all, in the advection phase before an X-point is created, currents form around the two separatrices that exist in this phase. Then, in the coronal reconnection phase, the strongest currents form around the X-point, creating a coronal BP via Ohmic heating. Weak currents build up also further along the two upper separatrices (which were the only separatrices in the first phase), as well as around the overlying field. The point-like brightening (the BP) is clearly accompanied by loop brightening.

Figure 3.6

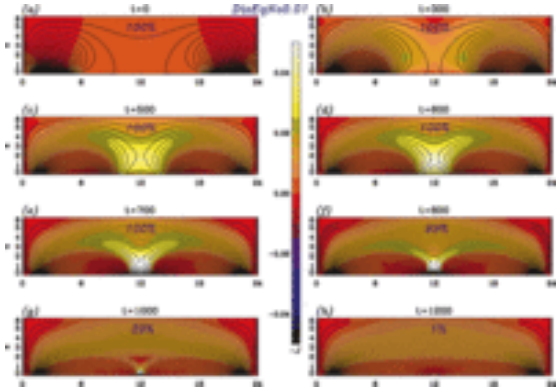

Magnetic field lines and current density (colours/grey shades) in Experiment DisEqNo0.01 with udriver= 0.01 at various times. The percentage values are same as in Fig.3.3.

Comparison:initially connected/disconnected bipole

BP lifetimes and cancellation times. In Experiment ConEqNo0.01, the coronal X-point phase (BP phase) goes from t= 0 until t≈ 400, that is, the BP lifetime is about 25 min. The CMF phase goes from t≈ 50 until t≈ 650, when 99 per cent of the vertical base flux in the inner bipole is cancelled, that is, the cancellation time is about 35 min. Hereby, ∼90 per cent of the flux is cancelled by the end of the BP phase. Both BP lifetime and cancellation time decrease roughly dynamically with increasing driving speed.

In DisEqNo0.01, the coronal X-point phase goes from t≈ 300 until t≈ 1150, that is, the BP lifetime is about 50 min (twice as long as in ConEqNo0.01). The CMF phase goes from t≈ 800 until t≈ 1200, when again 99 per cent of the vertical base flux in the inner bipole is cancelled, that is, the cancellation time is about 25 min (shorter than in ConEqNo0.01). Thus, cancellation starts here well into the BP phase (and also well after the maximum X-point height at t≈ 500–600), but as much as ∼95 per cent of the flux is cancelled by the end of the BP phase. Again, BP lifetime and cancellation time decrease roughly dynamically with increasing driving speed. It is noteworthy that in the 'Dis' experiments the ratio of 2 between BP lifetime and cancellation time is compatible with observations; absolute times are in the observed ranges when udriver≤ 0.004.

3.2. Reconnection of force lines of magnetic field

Magnetic reconnection is a physical process in highly conducting plasmas in which the magnetic topology is rearranged and magnetic energy is converted to kinetic energy, thermal energy, and particle acceleration. Magnetic reconnection occurs on timescales intermediate between slow resistive diffusion of the magnetic field and fast Alfvénic timescales.

Force-free equilibria and reconnection of the magnetic field lines in collisionless plasma configurations.

The plasma equilibrium in the force-free magnetic field in the framework of collisionless approximation is investigated. The equilibrium solution of the Vlasov–Maxwell equations, describing the distribution function of charged particles in the one-dimensional force-free magnetic field is obtained. It is shown that such a magnetic field can exist in plasma with anisotropic temperatures. Then, the tearing-mode instability of this configuration is investigated, and the results of 2D3V PIC (two coordinates and three velocity components particle-in-cell) simulations of the magnetic field lines reconnection during nonlinear development of the tearing-mode instability of the collisionless force-free equilibrium are presented.

Parker laid the foundation for the subject of magnetic reconnection in his fundamental early papers. We first of all summarise his contributions and give a new generalisation of the Sweet-Parker relations for a current sheet in which the outflow pressure is an extra parameter. Then we review the models for fast reconnection that have since been proposed, beginning with the Petschek mechanism and continuing to the more general Almost-Uniform and Nonuniform families. A comparison with numerical experiments is also made and the conditions under which fast reconnection exists are elucidated.

Extensive spatial and temporal measurements of plasma pressure nkTe, magnetic force density J × B, and ion velocities v have been performed in a laboratory experiment undergoing magnetic field line reconnection. The pressure is found to peak at the two edges of the neutral sheet. It exhibits large transverse gradients, causing space charge fields and Hall currents. The magnetic force density arises mainly from induced axial neutral sheet currents and transverse magnetic fields but also from transverse currents and a magnetic field component along the separator. The total force density on the fluid, J × B - ∇p, is compared with direct measurements of the fluid acceleration by using differential particle detectors. It is found that the ion acceleration is strongly modified by scattering off wave turbulence. After several Alfvén times the fluid

develops the classic flow pattern, with jetting from the edges of the neutral sheet to velocities close to the Alfvén speed.

3.3. Another mechanisms of flaring CBP

The mechanism of X-rays bright points appearance

The mechanism X-ray bright point production is simulated in the numerical MHD experiment. The anisotropy of plasma thermal conductivity in the magnetic field is taken into account. It is shown that plasma heating can be produced by magnetic line reconnection around the neutral line. The long time hot plasma confinement is provided by a magnetic trap configuration of the magnetic field.

There are two fundamental problems associated with X-rays bright points: the source of local heating of the corona, and long-time existence of very hot plasma (order of 10 hours) in a small restricted region in spite of high thermal conductivity of corona. Many observational data show that a X-rays bright point appears at emergence of a new weak magnetic flux. The velocity of magnetic flux emergence usually does not exceed 2 km/s. It is naturally to assume that plasma heating is produced by reconnection of emerged flux with the oppositely directed magnetic field in the vicinity of a neutral line. If the emerging flux is not too strong, all arriving magnetic field lines reconnect, but a powerful current sheet should not be produced.

For estimation the plasma cooling in a X-rays bright point the following parameters are used. The point diameter is d~5′ 108 cm, the plasma temperature is T~1000 eV, and the density is n~109 cm-3. The time of plasma cooling can be estimated from the equation: $\frac{\partial T}{\partial t} = \kappa_0 \frac{\partial^2 T}{\partial x^2}$. Here κ0=l2/tei ~1020T5/2/n, T is electron temperature in eV, n is plasma density in cm-3, l is the length of the electron free path, tei is the collision time for electrons. For these parameters κ0~3′ 1018, the time of cooling is t~d2/κ0 ~ 0.1s. The energy loss due to

thermal conductivity is W~nkTd3/t~1027 erg/s, and the energy output during typical time of XBP existence is about 1031 erg. This energy corresponds to a big solar flare.

These estimations contradict to observed data, because no drastic energy release is associated with a XBP. So, the mechanism of XBP should include a physical effect that reduces the thermal conductivity strongly. In the solar corona thermal conductivity reduction can be provided, if heat transport occurs across the magnetic field. Such conditions exist in the vicinity of a neutral line. The scenario of plasma heating and the hot plasma confinement around the neutral line of corona has been demonstrated in the preliminary numerical experiment in resistive MHD approximation for compressible plasma3. Here we present some new results. The new version of the PERESVET code is used. Calculations have been carried out for different magnetic field configurations with a neutral line and for different small photospheric disturbances. Here we present some new results. Strong anisotropy of thermal conductivity in the magnetic field is taken into account.

The results of calculations show that energy transference from the photosphere to vicinity of a neutral line occurs by magnetosound and Alfvenic waves. Magnetic field lines and distributions of velocity for t=0.1, 1.1, and 4.1 are shown in Fig. 1a, b, c.

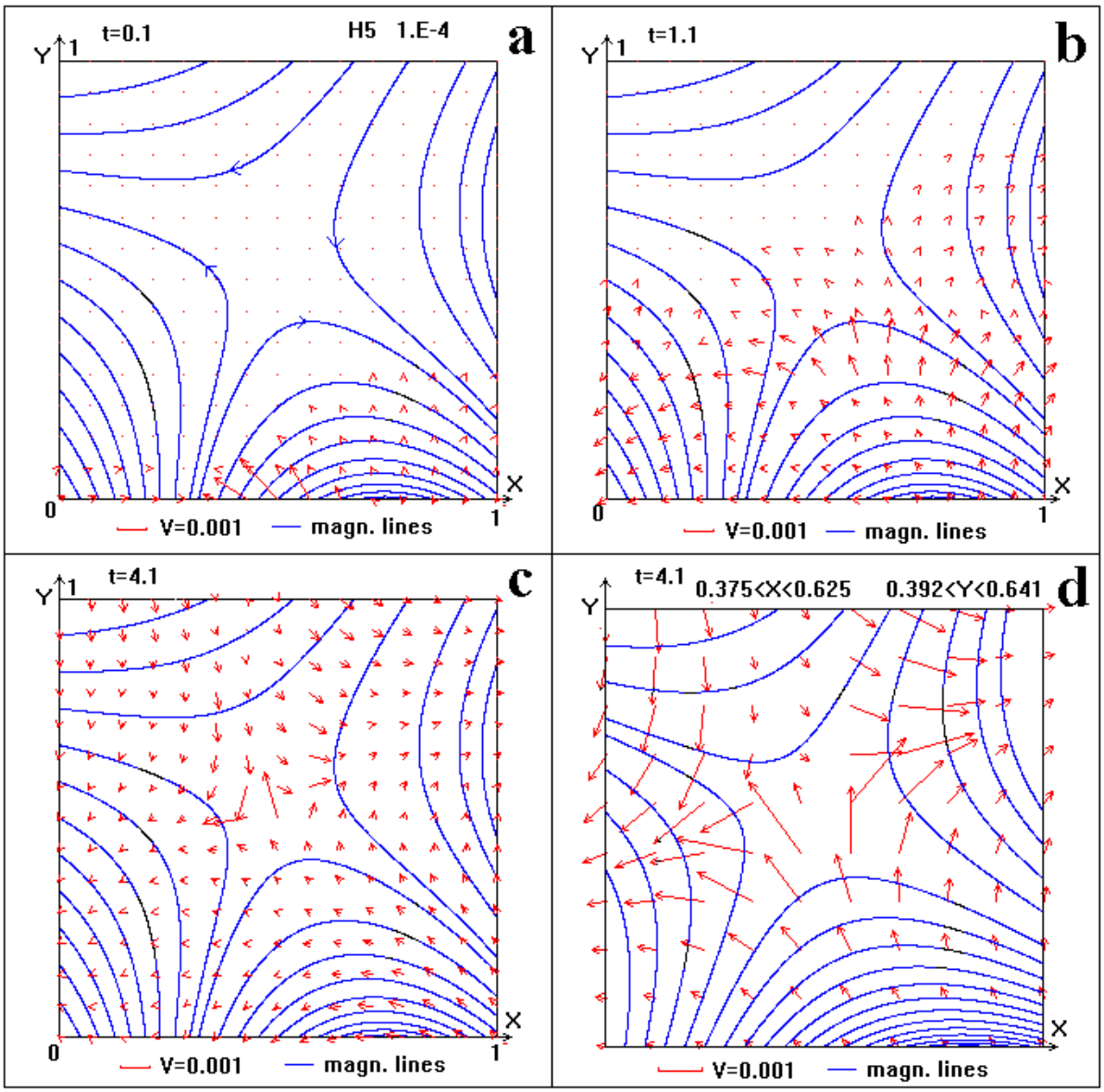

Figure 3.7. a) The distribution of the current density. b) Levels of r =cosnt. c) Distribution of the temperature. d) Magnetic field lines and levels of T=const (in the center). All data are presented for t=9.1.

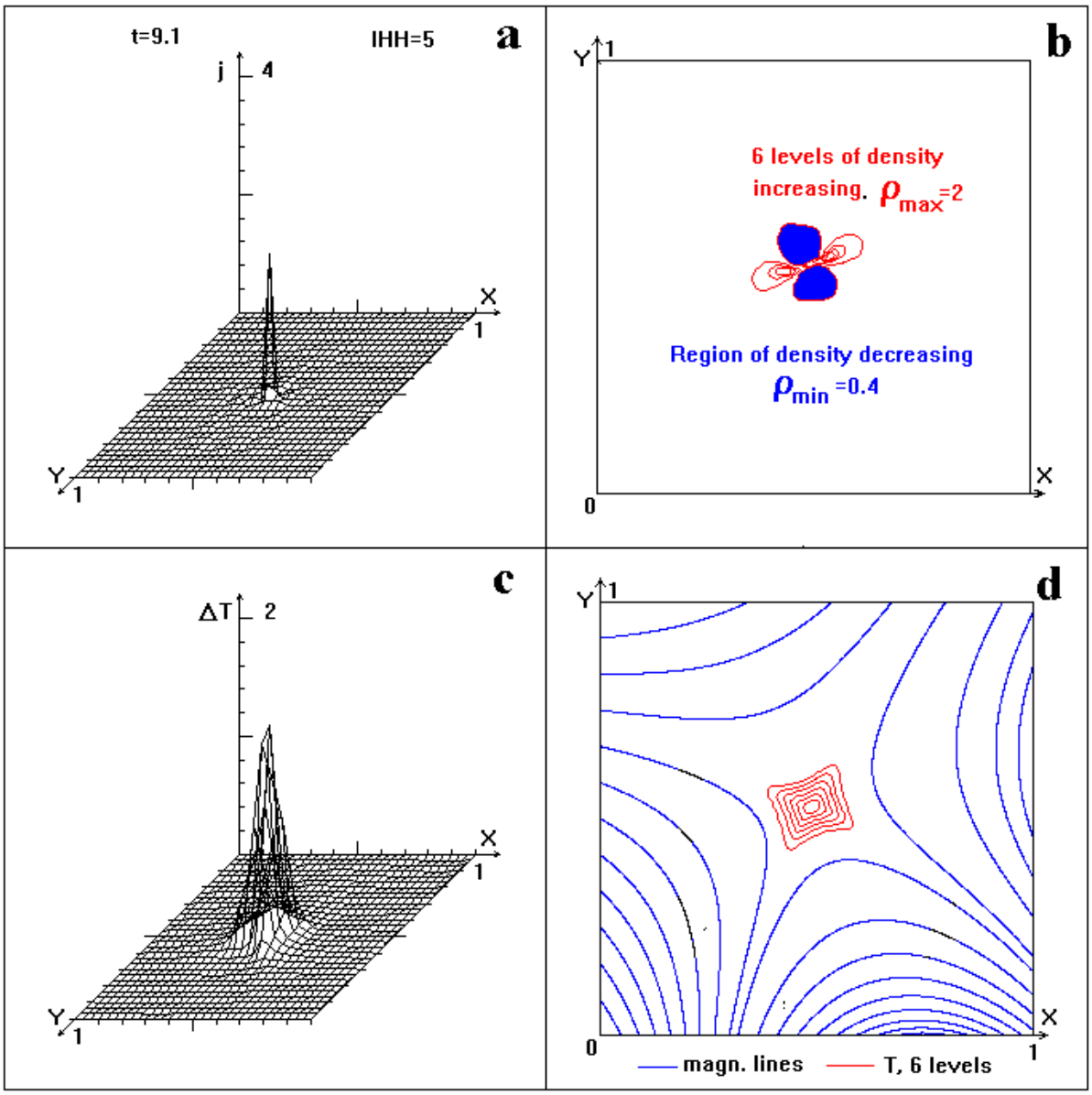

Figure 3.8

Apparently, X-ray bright points are responsible for solar cosmic rays generation during the minimum of solar activity, when the number of X-ray bright points increases by an order of magnitude8. At inflow velocity Vin = 0.001VA and B ~ 10 Gauss, the electric field along the neutral line is E = -VxB/c ~ 0.5 V/cm. If the point diameter is ~ 5*108 cm, the particle can be accelerated up to ~ 100 MeV.

CONCLUSION

In this study we use an automatic procedure to identify coronal bright points in EIT full disk images observed in the 195 A spectral range. We find a slight decrease of the total number of CBPs near the maximum of the sunspot cycle. We have divided the CBPs into two categories based on their maximum brightness, and we found opposite trends in cycle variation of dim and bright CBPs. Dim CBPs, associated with a quiet Sun, vary inversely with sunspot cycle, while the variation of bright CBPs (active Sun CBPs) shows a positive correlation with sunspot cycle in agreement with previous studies. The latitudinal distribution of dim CBPs suggests their uniform distribution over the Sun, while bright CBPs show an enhancement at latitudes associated with sunspot activity belts. We approximate cycle variation of dim and bright CBPs by Gaussian functions. The sum of these two functions shows a modest 30% dip around the maximum of the sunspot cycle, thus supporting the notion of inverse variation of CBP number with sunspot cycle. Finally, we argue that the decrease in number of dim CBPs at a solar maximum is caused mainly by the reduction in area of mixed polarity quiet Sun fields (because the area occupied by active regions increases at the solar maximum). In our opinion, the visibility effect, when the bright corona obscures CBPs, plays only an auxiliary role.

LIST OF USED LITERATURES

1. Ўзбекистон Республикасининг Конституцияси.- Т: Ўзбекистон. 1992-49 б.
2. Ўзбекистон Республикасининг "Кадрлар тайёрлаш миллий дастури" Баркамол авлод – Ўзбекистон тараққиётининг пойдевори.)-Т:Шарқ нашриёт матбаа- концерни.1997.-Б.31-61
3. Ўзбекистон Республикаси Олий таьлим муассаларида магистирлик дессертацияни тайёрлаш ҳакида НИЗОМ.- Т.:2008.-20б
4. Golub, L.; Davis, J.M.; Krieger, A.S. Anticoorelation of X-ray bright points with sunspot number, 1970-1978 // The ApJ, P. 2, 1979, v. 229, L. 145-150.
5. Шкловский И.С. Физика солнечной короны. 1962, Москва, Физматгиз, с. 82.
6. V. Domingo, B. Fleck, and A.I. Poland. The SOHO Mission: An Overviev.// Solar Phys.-1995.-V 162,No 1-2.-p. 1-37.
7. Саттаров И., Астрофизика курси, 1 ва 2 қисми, Молия иқтисод, Тошкент, 2008 ва 2009.
8. Прист Э.Р. Солнечная магнитогидродинамика. 1985 (пер с анг. ред. В.Н. Обритко), Москва, Мир, с.20
9. Пасачофф Дж. М. (J.M. Pasachoff), Solfr Eclipse Science. 2000. Sky & Telescope, No 2 p.4.
10. Zhang, J. et all, 2001, Solar Phys., V. 198, p. 347-365.
11. B.N. Handy, L.W. Acton, C.C. Kkankelborg, C.J. Wolfson, 48 co-authors, The Transition Region and Coronal Explorer.// Solar Phys. -1999.- V. 187, No 2.-h. 229-260.
12. Р.А.Сюняева. Физика.космоса. Маленкий.Энцеклопедия. Москва. 55б.1986
13. Кононович Э.В., Мороз В.И. Общий курс астрономии. Москва, УРСС, 2004 г.
14. V. Domingo, B. Fleck, and A.I. Poland. The SOHO Mission: An Overviev.// Solar Phys.-1995.-V 162,No 1-2.-p. 1-37.

15. Davis L., Krieger A., & Vaiana G. Solar Phys. -1975.-V. 42.-p.131.
16. I. Sattarov, A.A. Pevtsov, A.S. Hojaev and Ch. T. Sherdanov, X-ray bright points and photospyeric bipoles during cicles 22 and 23.// Astrophys. J.-2002a-V. 564, No2.-p/ 1042-1047.
17. Devis J.M. X-ray bright points and sunspot cycly: further results and predictions.// Solar Phys.-1983.-V 88, N ½.-p 337.
18. Tsuneta S., Acton L., Lemen J., Brown W., Caravalho R., Catura R, 36 co-authors. The Soft X-ray telescope for the SOLAR-A mission.// Solar Phys. -1991.-V.136.-p. 37.
19. Солнечного-Геофизическое Данные (Solar Geophysical data), Explanation issue. 1979-2001, No 500-700.
20. Сатаров И. и др. (I. Sattarov, A.S. Hojaev and Ch. T. Sherdanov), 3D-structure of the X-ray emitting regions/ 1997a, Proc. 31st ESLAB Symp., "Correlated phenomena at the Sun, in the Heliosphere and in Geospace", ESTEC, ESA SP-415, Noordwijk, The Netherlands, p. 387.
21. Эгамбердиев Ш.А. Исследование ярких рентгеновских точен на Солнце.-Дис. Канн. Физ.-мат Наук. Москва,1984.
22. S. Masuda, T. Kosugi, S. Tsuneta, Y. Ogawara, A loop-top hard X-ray source in compact solar flare as evidence magnetic reconnection.// Rep. from Nature.-1994.- V. 371, No 6497.-p. 495-497.
23. Шерданов Ч.Т., Тиллабоев А.М., Саттаров И., Карасчик Н.В. Солнечный ветер и яркие корональные точки, Сб. докладов II Республиканской конференции Молодых Физиков Узбекистана, 25-26 ноября, 2008, Ташкент, стр. 252-260.
24. Nina V. Karachik and Alexei A. Pevtsov, Solar wind and Coronal bright points inside coronal holes, Solar Phys. -2011.-V.735, No 47.-p.6-12.
25. www.umbra.nascom.nasa.gov/eit/eitcatalog.html.
26. Pevtsov, A. A., & Abramenko, V. I. 2010, in IAU Symp. 264, Solar and Stellar Variability: Impact on Earth and Planets, ed. A.G. Kosovichev, A. H. Andrei, & J.-P. Rozelot, 21.

DICTIONARY

English	Uzbek
1. **Sun**	**Quyosh**
2. Solar system	**Quyosh sistemasi**
3. Bright points	**Yorug' nuqtalar**
4. Magnetic field	**Magnit maydoni**
5. Evolution	**Evolutsiya**
6. Cycle	**Aylanish**
7. Ultraviolet	**Ultrabinafsha**
8. Solar corona	**Quyosh toji**
9. Polarity	**Qutblik, qarama qarshilik**
10. Plasma	**Plazma**
11. Chromosphere	**Xromosfera**
12. Eclipse	**Tutilish, xiralashish**
13. Observatory	**Observatoriya**
14. Satellite	**Suniy yo'ldosh**
15. Coronal structure	**Tojning tuzilishi**
16. X-ray	**Rentgen nuri**
17. Photosphere	**Fotosfera**
18. Solar wind	**Quyosh shamoli**
19. Wave energy	**To'lqin energiyasi**
20. Radiation	**Radiatsiya**
21. Magnetic flux	**Magnit oqimi**
22. Experiment	**Tajriba**
23. Emission	**Chiqarish, emissiya**
24. Interaction	**O'zaro tasir**
25. Sun watcher	**Quyoshni kuzatuvchilar**

26. Observe	**Kuzatmoq**
27. Equator	**Ekvator**
28. Rotation	**Aylanish, takrorlanish**
29. Latitude	**Kenglik**
30. Sidereal rotation	**Sedirik davr**
31. Hole	**Teshik**
32. Measure	**O'lchamoq**
33. Analyse	**Tahlil qilmoq**
34. Globe	**Globus**
35. Distribution	**Taqsimlash**
36. Investigate	**Tekshirmoq**
37. Angle	**Burchak**
38. Threshold	**Ostona, bo'sag'a**
39. Sunspot	**Quyosh dog'i**
40. Deviation	**Burilish, og'ish, nishab**
41. Distance	**Farq, oraliq**
42. Detector	**Qayt qilgich**
43. Dim	**Xira, rangi ketgan**
44. Activity	**Harakat**
45. Brightness	**Yorqinlik**
46. Axes	**Grafikdagi uqlar**
47. Map	**Xarita**
48. Intensity	**Intensivlik**
49. Connection	**Aloqa**
50. Atmosphere	**Atmosfera**